

Circumstellar features in hot DA white dwarfs

N.P. Bannister^{*1}, M.A. Barstow¹, J.B.Holberg², F.C.Bruhweiler³

¹*Department of Physics and Astronomy, University of Leicester, University Road, Leicester, LE1 7RH, U.K.*

²*Lunar and Planetary Laboratory, University of Arizona, Tucson, AZ 85721, USA*

³*Institute for Astrophysics & Computational Sciences (IACS), Department of Physics, The Catholic University of America, Washington DC 20064, USA*

Accepted YYYY MMMM DD. Received YYYY MMMM DD

ABSTRACT

We present a phenomenological study of highly ionised, non-photospheric absorption features in high spectral resolution vacuum ultraviolet spectra of 23 hot DA white dwarfs. Prior to this study, four of the survey objects (Feige 24, REJ 0457-281, G191-B2B and REJ 1614-085) were known to possess these features. We find four new objects with multiple components in one or more of the principal resonance lines: REJ 1738+665, Ton 021, REJ 0558-373 and WD 2218+706. A fifth object, REJ 2156-546 also shows some evidence of multiple components, though further observations are required to confirm the detection. We discuss possible origins for these features including ionisation of the local interstellar environment, the presence of material inside the gravitational well of the white dwarf, mass loss in a stellar wind, and the existence of material in an ancient planetary nebula around the star. We propose ionisation of the local interstellar medium as the origin of these features in G191-B2B and REJ 1738+665, and demonstrate the need for higher resolution spectroscopy of the sample, to detect multiple ISM velocity components and to identify circumstellar features which may lie close to the photospheric velocity.

Key words: stars:abundances – stars:atmospheres – stars:white dwarfs – circumstellar matter – ultraviolet:stars

1 INTRODUCTION

Spectral lines from highly ionised species are observed at non-photospheric velocities in several hot DO white dwarfs. Of the 11 stars included in the survey presented by Holberg et al. (1998) (hereafter referred to as HBS), six objects, all with temperatures $T_{\text{eff}} \geq 70,000$ K, were found to exhibit highly ionised features at non-photospheric velocities. Holberg et al. (1999) argue that such features cannot be of an interstellar origin since such highly ionised species are uncharacteristic of the local ISM, and are not observed along adjacent lines of sight to stars at greater distances. Further, while interstellar lines can be observed at velocities which are blue- or red-shifted with respect to the photospheric value v_{phot} , only blue-shifted features are found in the DO sample discussed by HBS. Such features provide strong evidence for the existence of ongoing mass loss in hot DO white dwarfs.

Although over 80% of known white dwarfs belong to the DA group (Sion et al. 1997), relatively few have been found to exhibit non-photospheric features. Only 5 of the 44 DA stars considered in HBS are accompanied by any type

of circumstellar feature, with no apparent dependence on temperature. In some instances, the appearance of this phenomenon can be plausibly explained in terms of interactions between binary components, as in the DA + dM 1.5 system Feige 24, which shows multiple components in the CIV $\lambda\lambda$ 1548, 1550 doublet.

However, in the DA white dwarf CD- 38° 10980, which is a member of a *wide binary* system, Holberg et al. (1995) find Si and C absorption features in IUE spectra, which are shifted by -12 km s^{-1} with respect to the photospheric velocity of the white dwarf, which can be inferred from its measured gravitational redshift. Holberg et al. showed that the atmosphere of this object was devoid of Si and C, at the expected photospheric velocity, and used the presence of excited or meta-stable levels in the shifted features as evidence that the material was not located in the ISM along the line-of-sight to the star. These observations were explained in terms of a dense, gaseous halo in close proximity to the star, possibly an extension to the atmosphere, for which a similar temperature and electron density was derived. Alternatively, Wolff et al. (2001) using FUSE observations of CD-38° 10980, observed a set of Si III lines shortward of 1120 Å which they attribute to the stellar photosphere. They were able to successfully model the observed equivalent widths

* Email: npb@star.le.ac.uk

of these lines as well as the Si lines seen in the IUE observations with a photospheric Si abundance of 2×10^{-8} . However, the velocity discrepancy remains unexplained. In another example of circumstellar features in an isolated DA object, Holberg et al. (1997) found evidence for weakly blue-shifted C IV and Si IV components in REJ 1614-085 ($T_{\text{eff}} \sim 38,500$ K) at $\approx 30\%$ of the strength of the photospheric lines, shifted by -25 and -40 km s^{-1} respectively. Similar features in the spectrum of the $T_{\text{eff}} \sim 57,000$ K DA, REJ 0457-289 have also been discussed by Holberg et al. (1997).

Agreement between the predicted and observed abundances of atomic species in the atmospheres of white dwarf stars has improved with the introduction of stratified model atmosphere codes, beginning with the stratification of He and Fe investigated by Barstow & Hubeny (1998) and Barstow et al. (1999). Dreizler & Schuh (2001) describe models in which stratified abundances are calculated self-consistently, by considering the depth dependence of temperature, density, radiation field and level populations using an iterative procedure. These models have succeeded in reproducing the soft X-ray, EUV and FUV spectra of a sample of DA stars, and can explain the widely varying levels of metallicity in hot DA white dwarfs. However, this agreement is not complete; for example, lines of C, N and O are not reproduced as accurately as those of Fe and Ni, while observed differences between objects of similar T_{eff} and $\log g$ are unexplained (Schuh & Dreizler 2001). The success of stratified models is encouraging, but the observation of highly ionised circumstellar features suggests the existence of processes which may modify the predicted equilibrium abundances, and improving the agreement between observed and predicted abundances requires better understanding of the nature of these features. It is particularly interesting that the DO white dwarfs, in which circumstellar features are relatively common, are also poorly modeled by the new generation of stratified codes (Dreizler & Schuh 2001).

Data from the *STIS* instrument on board HST have allowed the study of white dwarf spectra to be carried out with an accuracy impossible to achieve using earlier instruments, and at a resolution which permits more precise examination of intrinsic line profiles. A more sensitive search can now be made for signs of mass loss and accretion which may modify equilibrium abundances in white dwarf envelopes.

In section 2 we present a phenomenological study of a sample of 23 hot ($T_{\text{eff}} \geq 20,000$ K) DA white dwarf stars for which either *GHRs*, *STIS* or high resolution *IUE* echelle spectra were available. In each star, the resonance doublets of C IV, N V and Si IV have been examined for signs of multiplicity (whether in the form of asymmetry or distinct components), and statistical tests applied to determine the significance of proposed secondary features. In several stars, Gaussian profiles are used to model the observed lines. A Gaussian approximation to line data can be justified since, at the resolution of both the *IUE* echelle data ($R \approx 20,000$) and the *STIS* E140M grating ($R \approx 40,000$), unsaturated ISM lines are not resolved, nor are the photospheric profiles of most absorption lines. In some cases, elemental abundances are considered as additional evidence for the presence of non-equilibrium processes. The discussion of individual objects is divided into two subsections, covering stars which show clear (or suspected) highly ionised, non-photospheric fea-

tures, followed by those that do not *at the resolution of the data used in this study*. Several of the stars in this category exhibit unusual features which require further investigation at higher spectral resolution.

In section 3, the results of this study are discussed, and a variety of explanations for the presence of highly ionised non-photospheric features in certain white dwarfs, are considered.

2 OBSERVATIONS AND ANALYSIS

2.1 Observational data

The sample of stars was chosen to match that of Barstow et al. (2001), with the addition of the super-hot DA PG 0948+534 and Ton 021, since *GHRs*, *STIS* or high resolution *IUE* echelle spectra were available for these objects. Table 1 summarises the survey stars, their basic physical parameters, and the source(s) of data used in this work. Values for temperature and gravity were taken from Barstow et al. (2001). The adopted visual magnitudes were those of Marsh et al. (1997), except where otherwise stated. The mass, radius and distance to each star was estimated using the evolutionary models developed by Wood (1995), taking the stated values of T_{eff} , $\log g$ and m_v as input parameters.

The results of the survey are summarised in table 2, which includes the measured velocities of interstellar (v_{ISM}), photospheric (v_{phot}), and any non-photospheric highly ionised lines (v_{circ}) for all stars in the sample. Note that values for v_{circ} are not relative to the photospheric features, but are absolute velocities. Also included in the table are estimated values for the escape velocity (v_{esc}) and gravitational redshift (v_{grav}) of each star, and the velocity of the primary component of the local interstellar cloud along the line of sight to each star (v_{LIC}). As noted previously, the spectral resolution of *IUE*, *GHRs* and *STIS* (in the E140M configuration prevalent in this study) is insufficient to completely resolve the ISM components, and hence the value of v_{ISM} presented in table 2 represents the velocity of the primary component (or blend) observed in the data. This table also includes calculated values for gravitational redshift, escape velocity, and the velocity of the principal component of the local interstellar cloud in that direction. The local interstellar cloud can be described with reasonable accuracy by a cloud moving at 26 ± 1 km s^{-1} (heliocentric velocity) towards $l_{\text{II}} = (186 \pm 3)^\circ$, $b_{\text{II}} = (-16 \pm 3)^\circ$, or $\alpha = 74.5^\circ$, $\delta = +15^\circ$ (Lallement et al. 1995). The velocity of absorption lines from the LIC in a particular star, v_{LIC^*} , may be estimated from the projection of v_{LIC} onto the target direction.

2.2 Analysis methods

Absorption line parameters were measured using an IDL code, "Lines", written by one of us (JBH). The routine measures the properties (wavelength, velocity, equivalent width and associated uncertainties) of cursor-defined features in an input spectrum, given a user-supplied rest-frame wavelength for the feature. The principal lines in each spectrum were identified using the data contained in HBS, beginning with

Table 1. Stars included in the survey of circumstellar features, in descending temperature order. Mass, radius and distance calculated from the evolutionary models of Wood (1995). Visual magnitudes taken from Marsh et al. (1997) unless otherwise stated.

Star	T_{eff} (K)	$\log g$	M (M_{\odot})	R (R_{\odot})	m_v	D (pc)	Data source [Mode]	Resolution
PG 0948+534	90,000	7.27	0.478	0.027	13.71 ^e	193.8	<i>STIS</i> [E140M]	40000
REJ 1738+665	71,300	7.53	0.540	0.024	14.61	243	<i>STIS</i> [E140M]	40000
Ton 021	69,700	7.47	0.550	0.023	14.53 ^g	217	<i>STIS</i> [E140M]	40000
REJ 0558-373	63,000	7.66	0.580	0.019	14.37	295	<i>STIS</i> [E140M]	40000
REJ 2214-492	62,100	7.23	0.464	0.027	11.71	69	<i>IUE</i> [SWP]	20000
REJ 0623-371	59,700	7.00	0.399	0.033	12.09	97	<i>IUE</i> [SWP]	20000
WD 2218+706	56,900	7.00	0.396	0.033	15.40 ^c	436	<i>STIS</i> [E140M]	40000
Feige 24	56,400	7.36	0.546	0.021	12.56	78	<i>STIS</i> [E140M]	40000
REJ 2334-471	54,600	7.58	0.536	0.020	13.44	104	<i>IUE</i> [SWP]	20000
G191-B2B	54,000	7.39	0.510	0.021	11.73	50	<i>STIS</i> [E140M]	40000
GD 246	53,700	7.74	0.646	0.016	13.09	72	<i>STIS</i> [E140M]/ <i>IUE</i> [SWP]	40000/20000
REJ 0457-281	53,600	7.80	0.612	0.016	13.95	108	<i>IUE</i> [SWP]	20000
PG 1123+189	52,700	7.52	0.511	0.021	14.13	147	<i>STIS</i> [E140H]	110000
HZ 43	49,000	7.90	0.561	0.018	12.99	71	<i>IUE</i> [SWP]	20000
REJ 1032+532	46,300	7.78	0.585	0.016	14.46	127	<i>STIS</i> [E140M]	40000
REJ 2156-546	45,900	7.74	0.568	0.017	14.44	129	<i>STIS</i> [E140M]	40000
PG 1057+719	39,555	7.66	0.519	0.018	14.68 ^b	411	<i>GHR</i> [G160M]	22000
REJ 1614-085	38,500	7.85	0.596	0.015	14.01	86	<i>GHR</i> [G160M]	22000
GD 394	38,400	7.84	0.592	0.015	13.08	57	<i>IUE</i> [SWP]/ <i>GHR</i> [G160M]	20000/22000
GD 153	37,900	7.70	0.520	0.017	13.35 ^a	73	<i>IUE</i> [SWP]	20000
GD 659	35,300	8.00	0.662	0.013	13.37	53	<i>STIS</i> [E140M]/ <i>IUE</i> [SWP]	40000/20000
EG 102	20,200	7.90	0.573	0.014	12.76 ^d	25	<i>IUE</i> [SWP]	20000
Wolf 1346	20,000	7.90	0.572	0.014	11.52 ^f	14	<i>IUE</i> [SWP]	20000

^a Bohlin et al. (1995)

^b Holberg et al. (1997)

^c Napiwotzki & Schönberner (1995)

^d Greenstein (1984)

^e Holberg et al. (1995)

^f Dahn et al. (1988)

^g Saffer et al. (1998)

Table 2. Measured velocities for interstellar, photospheric and non-photospheric lines for surveyed stars. Tentative identifications are marked “?”. All velocities in km s^{-1} .

Star	v_{esc}	v_{grav}	v_{LIC}	v_{ISM}	v_{phot}	v_{circ}
PG 0948+534	2645	11.3	10.00	-0.26 ± 1.26	-14.25 ± 0.22	
REJ 1738+665	3365	14.2	-3.46	-18.56 ± 0.09	30.19 ± 0.27	-17.80 ± 0.33
Ton 021	3074	15.2	10.61	0.86 ± 0.01	37.14 ± 0.21	7.62 ± 1.27
REJ 0558-373	3477	19.6	25.19	11.61 ± 1.40	22.74 ± 2.81	7.15 ± 0.77
REJ 2214-492	2526	10.9	-8.54	-1.72 ± 0.51	33.49 ± 0.45	
REJ 0623-371	2143	7.7	14.46	16.40 ± 0.70	41.15 ± 0.56	
WD 2218+706	2143	7.6	4.93	-10.11 ± 0.19	-38.69 ± 0.23	-16.34 ± 0.67
Feige 24	2588	17.0	20.52	8.22 ± 0.10	80.33 ± 0.50	$\Delta V = 25.0 \pm 3.5$
REJ 2334-471	3253	17.0	-2.62	15.15 ± 1.52	40.57 ± 2.07	
G191-B2B*	2679	15.4	20.58	8.6	25.20 ± 0.26	7.56 ± 0.19
GD 246	3498	25.7	2.40	-5.78 ± 0.12	-13.29 ± 0.25	
REJ 0457-281	3749	24.3	18.92	14.48 ± 2.15	76.91 ± 0.83	21.76 ± 1.27
PG 1123+189	3111	15.5	-0.36	-0.67 ± 0.06	12.55 ± 0.53	
HZ 43	4461	19.8	-8.83	-16.86 ± 2.07	—	
REJ 1032+532	3663	23.3	7.41	0.84 ± 0.21	38.16 ± 0.40	
REJ 2156-546	3606	21.2	-9.65	-8.39 ± 0.18	-19.94 ± 0.68	-1.65 ± 0.76 ?
PG 1057+719	3384	18.3	6.51	-2.89 ± 0.69	75.35 ± 2.59	
REJ 1614-085	3845	25.3	-25.29	-29.56 ± 0.33	-37.31 ± 0.40	-71.42 ± 6.63
GD 394	3801	25.1	-2.16	-7.28 ± 1.42	28.75 ± 0.91	
GD 153	3444	19.4	-8.65	-8.42 ± 2.68	12.45 ± 2.07 ?	
GD 659	4254	32.4	6.12	9.77 ± 0.22	34.28 ± 0.17	-2.97 ± 3.00 ?
EG 102	3934	26.0	1.05	-1.37 ± 3.85	-0.69 ± 1.44	
Wolf 1346	3934	26.0	-10.76	-15.38 ± 0.95	24.32 ± 1.41	

*ISM velocity from Sahu et al. (1999); no error quoted. Value for ISM velocity determined from current work (using lower resolution data) is $v_{\text{ISM}} = 16 \pm 1 \text{ km s}^{-1}$.

unambiguous features such as the saturated interstellar lines of, e.g., N I, and the resonance doublets of photospheric CIV and SiIV. Subsequent identifications were validated against the resulting ISM or photospheric velocity.

Gaussian line profiles have been fitted to observed features to determine the velocity of circumstellar material, or multiple ISM clouds along the line-of-sight. The profiles were fitted using further bespoke IDL routines which applied first a single, and then dual, Gaussian to cursor-identified features in the spectra via the χ^2 minimisation technique, generating values for the velocity and equivalent width of the best-fit components. In cases where the dual-Gaussian fit was not obviously superior, χ^2 values from the single and dual fits were then used to perform a standard *F*-test, following the method outlined by Holberg et al. (1997), to determine whether a significantly better fit to observation was obtained with the latter.

In addition to the IDL routines, cross-checking of results was performed using the *Dipso* package (part of a suite of tools produced for the UK *Starlink* system). Excellent consistency was observed between results obtained from these disparate packages.

Co-addition of spectral features has been performed in several cases in order to reveal details which are only marginally detectable at the S/N of the data. In this technique, $\sim 10 \text{ \AA}$ - wide sections of spectral data are extracted, each centered on the wavelength of a particular line of a given species (e.g. the $\lambda\lambda 1548, 1550$ lines of CIV). The sections are then transformed into velocity space so that each shows a line at the velocity of the primary interstellar cloud or the photosphere. Spectral sections are then co-added so that the strength of the (randomly distributed) noise features remains essentially unchanged, while absorption features sharing a common velocity are summed. The result is a spectrum with improved S/N, showing the profile of lines of a particular species.

Co-addition does not improve the resolution of the data, and is therefore ineffective in revealing circumstellar features which are blended with their photospheric counterparts at the resolution of the data. Further, the technique is only effective when several of the primary lines are accompanied by such features. Nevertheless, co-addition has proved to be a useful technique in detecting weak circumstellar features which are clearly separated from the primary component at the resolution of the instrument.

2.3 Comments on individual objects

2.3.1 Stars exhibiting circumstellar features

REJ 1738+665

REJ 1738+665 is the hottest DA white dwarf to be detected by *ROSAT* (Barstow et al. 1994b). A photospheric velocity of $v_{\text{phot}} \approx 30 \pm 1 \text{ km s}^{-1}$ is determined, based on absorption features arising from Fe, Ni and O which show no multiple components; interstellar lines indicate a line of sight ISM velocity of $v_{\text{ISM}} \approx -18 \pm 1 \text{ km s}^{-1}$. The line of sight velocity of the LIC is estimated to be $v_{\text{LIC}^*} \approx -3.4 \text{ km s}^{-1}$.

Clear evidence is found for the presence of circumstellar material in this star. Figure 1 shows the CIV resonance doublet in REJ 1738+665, with shifted components at $-18.5 \pm 0.5 \text{ km s}^{-1}$ dominating the 30 km s^{-1} photo-

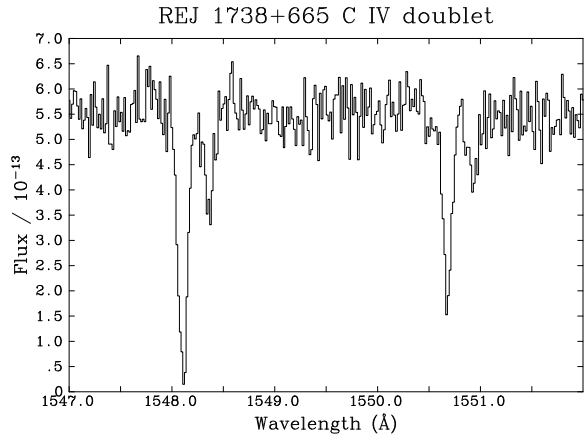


Figure 1. Clear multiplicity in the C IV doublet of RE 1738+665, with the photospheric components dominated by the blueshifted lines.

spheric contribution. Shifted features with similar velocities are observed in several other species, although in each case the photospheric component is dominant. The SiIV doublet shows non-photospheric components at $-17.7 \pm 0.7 \text{ km s}^{-1}$. Viewed individually, the lines of the NV doublet ($\lambda\lambda 1238.821, 1242.804$) show no evidence of companions, but co-addition of these features suggests an extra, weak component at $-15.2 \pm 2 \text{ km s}^{-1}$. The OIV doublet ($\lambda\lambda 1338.612, 1343.512$) shows no additional features, but the OV line at $\lambda 1371.292$ is accompanied by a weak shifted component at $-18.7 \pm 0.5 \text{ km s}^{-1}$. Curve-of-growth analysis of the CIV and SiIV lines indicate column densities of N (CIV) = $1.70 \times 10^{13} \text{ atoms cm}^{-2}$ and N (SiIV) = $1.66 \times 10^{13} \text{ atoms cm}^{-2}$ with $b \approx 5 \text{ km s}^{-1}$ (curves for the SiIV features are shown in figure 2).

The velocities measured for these shifted features differ from v_{ISM} by less than 0.75 km s^{-1} . This raises the possibility that they may be produced by photoionisation of the ISM within the Strömgren sphere around the star. However, Tweedy & Kwitter (1994) also present evidence for the possible existence of a planetary nebula around the star, based on the observation of N II circumstellar features at optical wavelengths. The non-photospheric features of REJ 1738+665 may therefore be produced by ionisation of the ancient planetary nebula remnant surrounding this star. The relationship between planetary nebulae and highly ionised non-photospheric lines is discussed in section 3.

Ton 021

Other than its inclusion in general white dwarf surveys, Ton 021 has received comparatively little attention in the literature. We determine $T_{\text{eff}} = 69700 \pm 530 \text{ K}$ and $\log g = 7.47 \pm 0.05$ (c.f. 69711 ± 1030 and 7.469 ± 0.05 respectively from Finley et al. (1997)). Weighted averages of the significant interstellar and photospheric absorption features give values of $v_{\text{ISM}} = 0.86 \pm 0.01 \text{ km s}^{-1}$ and $v_{\text{phot}} = 37.25 \pm 0.22 \text{ km s}^{-1}$. Among the observed interstellar features are strong lines of C II at $\lambda 1334.5323$ (equivalent width $171 \pm 1.6 \text{ m\AA}$) and $\lambda 1335.7076$ (equivalent width $61 \pm 2.2 \text{ m\AA}$). Velocities consistent with the weighted average v_{ISM} are observed for the broad interstellar lines of N I and Si II; however, the

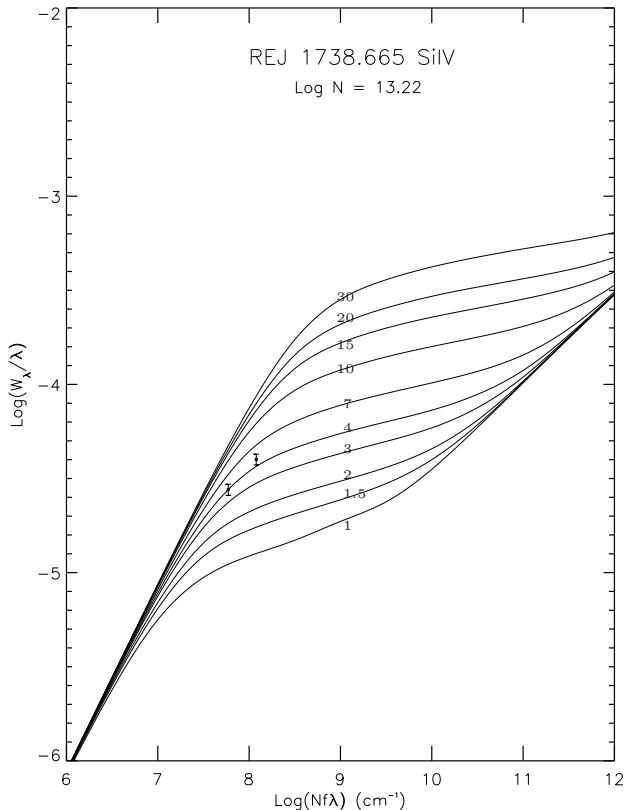


Figure 2. Curves of growth for Si IV in REJ 1738+665. Separate curves in each plot correspond to different values of the Doppler parameter, b (indicated in km s^{-1}).

Si III $\lambda 1206.5$ line appears at $7.8 \pm 0.7 \text{ km s}^{-1}$. This is not a unique observation; Holberg et al. (1999a) find significant differences between the velocity of this line and the mean value of v_{ISM} in REJ 1032+532 (also included in the current study). Holberg et al. discuss this observation in some detail, arguing that the Si III feature is unlikely to originate in the LIC due to the high ionisation fraction of hydrogen ($\sim 95\%$) required to maintain detectable amounts of Si III, which has a high rate coefficient for charge exchange with neutral H. As noted by Holberg et al. (1999a), a similar observation is made by Vidal-Madjar et al. (1998) in the case of G191-B2B.

Both lines of the CIV resonance doublet are accompanied by shifted features. In the $\lambda 1548.202$ line, the non-photospheric component is best fit by a Gaussian with a velocity of $v_{\text{circ}} = 9.5 \pm 1.0 \text{ km s}^{-1}$, and an equivalent width of $20 \pm 5 \text{ m}\text{\AA}$. This velocity agrees, within the stated error margin, with that determined for the Si III line. The shifted component in the $\lambda 1550.774$ line is fit by a Gaussian at $v_{\text{circ}} = 5.5 \pm 2.2 \text{ km s}^{-1}$, with an equivalent width of $9.4 \pm 2.5 \text{ m}\text{\AA}$. The estimated CIV column density contributing to these shifted features is $N(\text{CIV}) = 3.98 \times 10^{12} - 1.26 \times 10^{13} \text{ atoms cm}^{-2}$ based on a curve-of-growth analysis. In both cases, the photospheric components are found at velocities consistent with the average value for v_{phot} . The presence of a non-photospheric CIV feature is most clearly demonstrated in the co-added lines of the resonance doublet, as shown in figure 3.

Viewed individually, the lines of the Si IV resonance

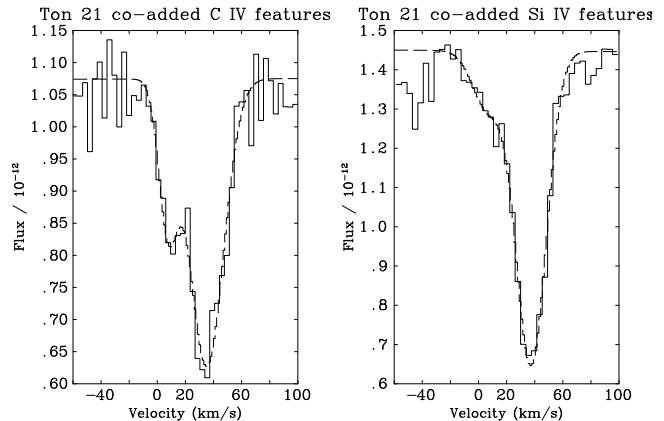


Figure 3. The co-added C IV and Si IV resonance lines of Ton 021. Clear evidence for multiplicity is observed in the C IV features, while the presence of a non-photospheric component to the Si IV features is less compelling. Dotted line: best fit dual-Gaussian to the data.

doublet appear slightly asymmetrical but show no clear multiplicity at the resolution of this data. When co-added, this asymmetry is more noticeable (as shown again in fig 3), and we find the best fit dual-gaussian to be one with a primary component at $\sim 37 \pm 1.2 \text{ km s}^{-1}$, in agreement with v_{phot} , and a non-photospheric component at $\sim 6.5 \pm 12.3 \text{ km s}^{-1}$. Although this velocity is close to the value of v_{circ} found in the CIV doublet, there is considerable uncertainty in the measurement, and data of higher S/N will be required to confirm the detection of non-photospheric components to the Si IV doublet of Ton 021.

REJ 0558-373

The CIV $\lambda\lambda 1548.202, 1550.774$ lines in this star are moderately asymmetrical. An F -test suggests that a dual Gaussian fit is preferred over a single line, above the 98% confidence interval, for each feature. No corresponding asymmetries are observed elsewhere in REJ 0558-373.

For the $\lambda 1548.202$ line, the individual components are found at 7.0 ± 1.0 and $26.8 \pm 1.2 \text{ km s}^{-1}$ (with equivalent widths of 79 and 68 $\text{m}\text{\AA}$ respectively). Corresponding values for the $\lambda 1550.774$ line are 7.9 ± 1.2 and $21.8 \pm 1.0 \text{ km s}^{-1}$ (13 $\text{m}\text{\AA}$ and 150 $\text{m}\text{\AA}$). Fits to each line are illustrated in figure 4. For comparison, $v_{\text{phot}} = 22.7 \pm 2.8 \text{ km s}^{-1}$, and $v_{\text{ISM}} = 11.6 \pm 1.4 \text{ km s}^{-1}$, and hence the longer wavelength component of each CIV line is in reasonable agreement with the photospheric value.

v_{grav} is estimated as $\approx 20 \text{ km s}^{-1}$ for this star, which is greater than the $\sim 10 \text{ km s}^{-1}$ difference between the photospheric and shifted CIV components. It is therefore possible that the blueshifted, non-photospheric CIV features could be formed by material *within* the potential well, rather than the weakly shifted outer regions. However, the non-photospheric components lie close to the velocity of the ISM, raising instead the possibility that the star is ionising material in its local interstellar environment. In either case, the absence of corresponding features in other strong lines is puzzling.

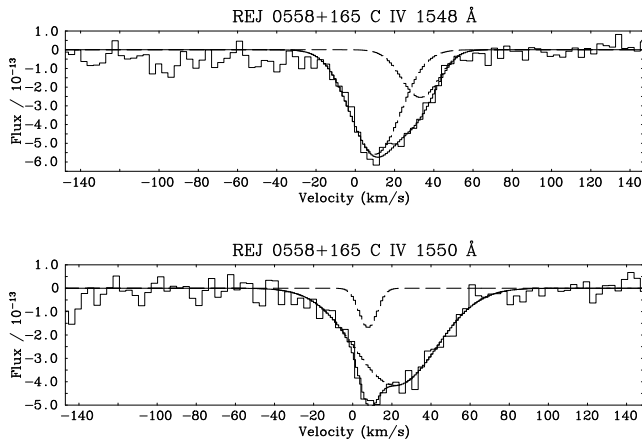


Figure 4. Lines of the C IV doublet of REJ 0558-373, in velocity space, with Gaussian fits overlaid (histogram = *STIS* data; dashed curves: component Gaussians; solid curve: compound fit).

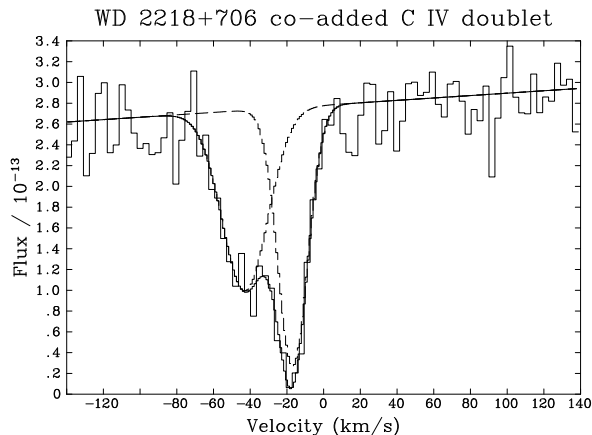


Figure 5. Histogram: co-added lines of the C IV doublet in WD 2218+706 showing the photospheric component at 38.8 km s^{-1} , accompanied by a redshifted feature at -16.3 km s^{-1} . The data are accompanied by the individual and summed components of the best-fit dual Gaussian.

WD 2218+706

This object is unusual and important in several respects. Lines of the C IV and Si IV doublets are clearly multiple, dominated by a photospheric contribution, but with accompanying components of comparable equivalent width at a velocity of $-16.3 \pm 0.7 \text{ km s}^{-1}$. These features are therefore *redshifted* with respect to the photospheric velocity ($v_{\text{phot}} = -38.7 \pm 0.2 \text{ km s}^{-1}$), possibly representing the infall of material onto the white dwarf. Gravitational redshift therefore provides no viable explanation for these lines.

WD 2218+706 is surrounded by an old planetary nebula, DeHt5, and is discussed by Napiwotzki & Schönberner (1995). In a study of planetary nebula dynamics, Dgani & Soker (1998) show that in regions where the ISM is reasonably dense (such as the galactic plane), Rayleigh-Taylor instabilities can develop in the outer regions of planetary nebulae, leading to fragmentation of the halo, and allowing the surrounding ISM to pass into

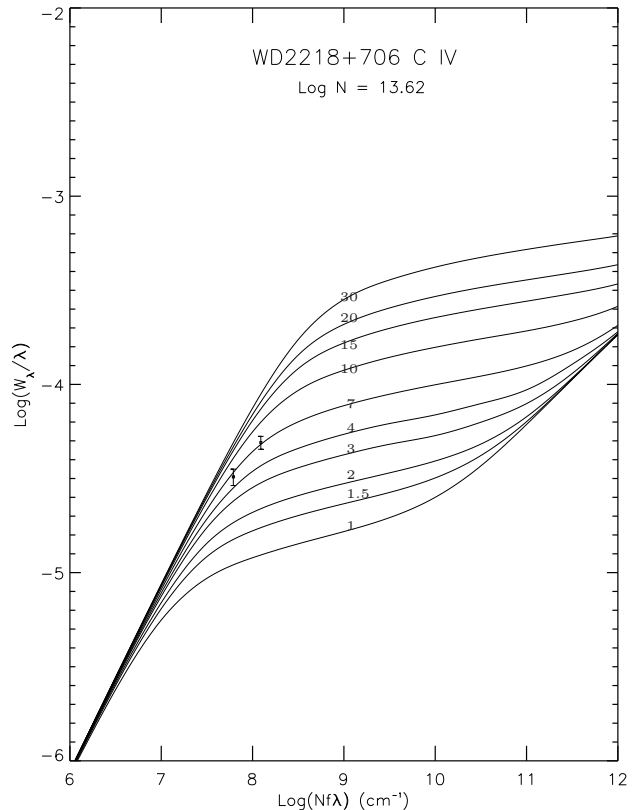


Figure 6. Curves of growth for the redshifted C IV features in WD 2218+706. Separate curves in each plot correspond to different values of the Doppler parameter, b (indicated in km s^{-1})

the inner regions of the nebula where photoionisation can occur. Although WD 2218+706 is out of the galactic plane ($b_{\text{II}} = 11.6^\circ$), and therefore lies in a region where the mean ISM density may be expected to be relatively low, Kun (1998) describes the morphology of a nearby giant molecular cloud complex consisting of a large number of distinct regions previously identified in independent surveys; several are found close to WD 2218+706, and two are of particular interest (Lynds 1217 and Lynds 1219). The central portions of these clouds have galactic coordinates within less than 0.5° of this star, and their distance limits (from 380 to 450 pc) encompass the distance to WD 2218+706 (440 pc, from Napiwotzki & Schönberner). This raises the possibility that the star may lie in an area where the ISM is particularly dense, allowing instability and inflow to take place (a curve of growth analysis for the non-photospheric features in WD 2218+706 suggests column densities of $N(\text{C IV}) = 4.17 \times 10^{13} \text{ atoms cm}^{-2}$ and $N(\text{Si IV}) = 4.07 \times 10^{13} \text{ atoms cm}^{-2}$, each with a Doppler parameter of 6 km s^{-1}). However, alternative explanations, such as the presence of a hidden companion, are also deserving of investigation, and this work is currently in progress.

During the course of the WD 2218+706 study, evidence was found for the existence of trace amounts of He in the *STIS* spectrum (Barstow et al. 2001), with the He II $\lambda 1640.5050$ line observed in the *STIS* spectrum close to the estimated photospheric velocity. As noted by Barstow et al., the $\lambda 1640.5050$ line has an $n=2$ lower level, which should not be populated in collisionless interstellar material, while any

helium in the surrounding planetary nebula would be expected to be found in emission. Hence a photospheric origin appears to be the most satisfactory of these three possible sources. The surface gravity of WD 2218+706 ($\log g \approx 7.00$) is low for an isolated white dwarf, and may be explained in terms of close-binary evolution, in which the progenitor star fills its Roche lobe and loses mass to a companion. This loss of material prevents helium ignition from taking place. Instead, the star, consisting of a He core surrounded by a H-rich envelope (which still supports nuclear reactions at the base), contracts slowly towards the low-mass, He-core white dwarf configuration (Driebe et al. 1998; Napiwotzki 1999). As the case of Feige 24 illustrates, the presence of a binary companion can contribute to the appearance of circumstellar lines. However, there is no direct evidence for the existence of a binary companion, and the range of possible masses for this star does not preclude AGB evolution, leaving open the possibility that WD 2218+706 is the product of single-star evolution.

Evidence exists for at least one other H-rich white dwarf star exhibiting the He II $\lambda 1640$ line, in the DAB HS 0209+0832 ($T_{\text{eff}} \sim 35,000$ K; $\log g \sim 7.8$). This star is discussed by Wolff et al. (2000), who suggest that significant quantities of He are present in the atmosphere, despite the short diffusion timescales for He, as a result of ongoing accretion of matter from an interstellar cloud. Supporting evidence for this explanation can be found in the work by Heber et al (1997), who observe variability in the strength of the He $\lambda 1640$ line, possibly as a result of the passage of HS 0209+0832 through an inhomogeneous medium. Alternatively, Unglaub & Bues (2000) find that DAO stars, in which mass loss in the form of a stellar wind prevents He from sinking out of the atmosphere, can transform into DA stars when the phase of wind-driven mass loss ends. This transition is found to occur near $\log g \sim 7.0$ for a star with $T_{\text{eff}} \sim 60,000$ K (see fig.6, Unglaub & Bues (2000)), raising the possibility that WD 2218+706 may be such a transitional object.

Feige 24

Feige 24 is a white dwarf+red dwarf binary system, and is the subject of several detailed studies (e.g. Dupree & Raymond 1982; Vennes & Thorstensen 1994). Two *STIS* data-sets were available for this star, acquired on November 29th 1997 (binary phase 0.73–0.75) and January 4th 1998 (binary phase 0.23–0.25), representing the orbital quadrature points. Vennes & Thorstensen estimate a systemic velocity of 62.0 ± 1.4 km s⁻¹. For the current study, the systemic velocity has been estimated by taking the mean of the photospheric values obtained from each data set (31.6 and 129.1 km s⁻¹), resulting in an estimated systemic velocity of 80.3 ± 0.5 km s⁻¹. v_{ISM} is estimated at 8.2 ± 0.1 km s⁻¹.

Feige 24 is known to exhibit multiple components, in the lines of the CIV doublet only. In this work, the dominant components match the photospheric velocity of each data-set, and secondary features are observed to remain at 7.8 ± 0.2 km s⁻¹, irrespective of the orbital phase. This stationary component has been discussed by Dupree & Raymond, who suggest that the most likely source is a Strömgren sphere excited by the white dwarf, and measure column densities of

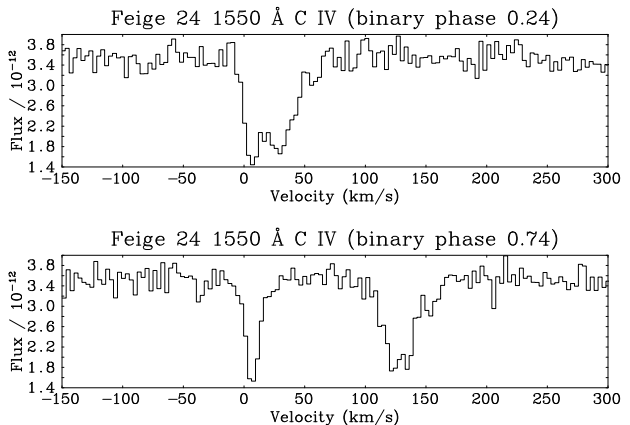


Figure 7. The C IV 1550 Å feature of Feige 24 as observed at the two quadrature points. The stationary circumstellar component is clearly visible, as is the orbital velocity of the photospheric component.

$N(\text{CIV}) = 3.86(\pm 1.51) \times 10^{13}$ atoms cm⁻² using curves-of-growth. Vennes & Thorstensen investigated the possibility that the material responsible resides in the photosphere, in a circumstellar shell, or in a wind from the red dwarf companion. The current study shows no shifted components in any of the other resonance lines (e.g. Si IV or NV). A *third*, very weak feature on the red side of each photospheric line in the CIV doublet, most obviously at 1550 Å, is identified as the Fe V $\lambda 1550.907$ line.

The gravitational redshift estimate made during this study, $v_{\text{grav}} \approx 17$ km s⁻¹, is somewhat higher than that derived by Vennes & Thorstensen ($v_{\text{grav}} \approx 9 \pm 2$ km s⁻¹), but is still too low to explain the secondary CIV components. However, their velocities agree, within error, with that of the ISM, and hence a link between the star and its immediate surroundings (beyond any circumstellar shell) cannot be discounted. Alternatively, Vennes & Thorstensen estimate that a CIV column density from $N(\text{CIV}) = 7.94 \times 10^{11} - 7.94 \times 10^{13}$ atoms cm⁻² (corresponding to equivalent widths of between 4–400 mÅ for the non-photospheric component of the $\lambda 1550.774$ line, assuming a linear curve-of-growth), would be consistent with mass loss from the red dwarf companion. Although insufficient data are available to derive an unambiguous CIV column density in this study, the estimated value of $N(\text{CIV}) = 1.48 \times 10^{13}$ atoms cm⁻², is within the range of possible values obtained by Vennes & Thorstensen, and the equivalent width of the $\lambda 1550.774$ line (24 mÅ) is also consistent with the large range allowed by earlier estimates.

G191-B2B

The *STIS* E140M data for this star show the CIV resonance doublets are accompanied by strong non-photospheric blue shifted components, confirming the results of Bruhweiler et al. (1999). The wavelength and equivalent width of these features have been estimated by fitting multiple Gaussians to the data, as shown in figure 8. The component at photospheric velocity is of greater equivalent width, and the shifted elements are observed at velocities of 7.6 ± 0.2 km s⁻¹. Recently, Holberg et al. (2002) also detected weak blue shifted components to the Si IV

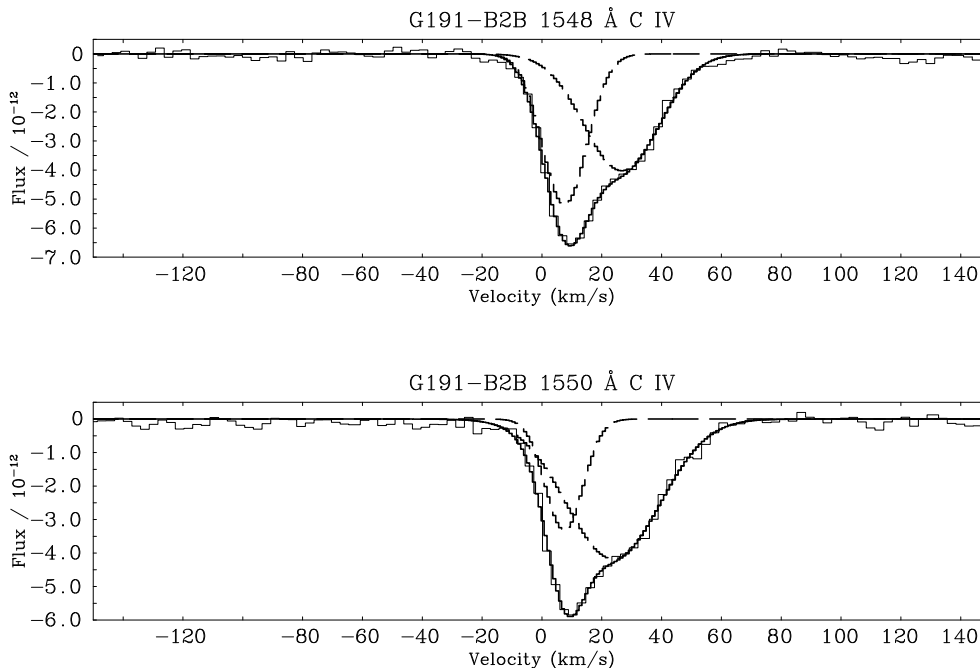


Figure 8. The C IV doublet of G191-B2B, in velocity space, with compound Gaussian fits (solid lines), and the individual Gaussian components (dashed lines).

$\lambda\lambda 1393.755, 1402.777$ doublet at the same velocity as the non-photospheric C IV features, using 22 co-added *STIS* E140H spectra.

The calculated figure of $v_{\text{grav}} \approx 15.4 \text{ km s}^{-1}$ is comparable with the velocity difference between photospheric and shifted high ionisation features, suggesting that the non-photospheric material probably resides outside the limit of the potential well. The velocity of the highly ionised non-photospheric features is substantially different to the value of the interstellar features ($v_{\text{ISM}} = 16 \pm 1 \text{ km s}^{-1}$ as determined in this work), and at first sight, photoionisation of the cloud responsible for the primary ISM features does not appear to provide a viable explanation. However, the value quoted for v_{ISM} is based on analysis of an E140M (medium resolution) *STIS* data-set, with a resolving power of ~ 35000 . Sahu et al. (1999) describe observations made with the E140H grating (resolving power ~ 110000), and clearly show *two* distinct interstellar components, with velocities of $\sim 8.6 \text{ km s}^{-1}$ and $\sim 19.3 \text{ km s}^{-1}$, the latter component having a velocity close to the predicted value of v_{LIC} (estimated at 20.58 km s^{-1} in this study). Clearly, the highly ionised non-photospheric components have a velocity which is very close to the 8.6 km s^{-1} interstellar cloud.

A curve-of-growth analysis was performed for the C IV features in G191-B2B. As in the case of Feige 24, the availability of only two datum points prevents any rigorous constraints from being placed on the implied C IV column density, though the value of $N(\text{C IV}) = 2.40 \times 10^{13} \text{ atoms cm}^{-2}$ is not dissimilar from the results of Vennes & Lanz (2001), who use synthetic modeling techniques to estimate a value of $N(\text{C IV}) = 6.31 \times 10^{13} \text{ atoms cm}^{-2}$. The Doppler parameter suggested by the current analysis, $b = 10 \text{ km s}^{-1}$,

is significantly higher than the value of $b = 5.2 \text{ km s}^{-1}$ presented by Vennes & Lanz; this discrepancy may also be explained by the lack of available data in the current work.

REJ 0457-281

The exceptionally low HI column density to this star ($1.3 \times 10^{17} \text{ atom cm}^{-2}$), was revealed in the discovery paper by Barstow et al. (1994a). Along with G191-B2B, this white dwarf was the first to have phosphorous and sulphur identified in its spectrum (Vennes et al. 1996). Later, HBS showed that the photospheric Si IV and C IV resonance lines of REJ 0457-281 are accompanied by blue-shifted features (figure 9).

Few interstellar and photospheric lines are identifiable, making precise velocity measurements difficult. The ISM velocity estimate of HBS is confirmed, but somewhat higher photospheric velocities are derived. Co-addition of the C IV doublet lines clearly reveals two velocity components: one at $22.5 \pm 1.39 \text{ km s}^{-1}$, and the photospheric component at $81.26 \pm 2.65 \text{ km s}^{-1}$. A curve of growth analysis for the non-photospheric components suggests $N(\text{C IV}) \sim 1.82 \times 10^{14} \text{ atoms cm}^{-2}$ with a Doppler parameter $b \approx 4 \text{ km s}^{-1}$. For the co-added Si IV doublet, corresponding velocities are $19.08 \pm 4.31 \text{ km s}^{-1}$ and $80.65 \pm 1.38 \text{ km s}^{-1}$. Although multiple velocity components are not obvious in the NV doublet, there is, nevertheless, evidence to suggest that they are present (figure 9). The $\lambda 1238.8210 \text{ NV}$ line is a narrow, well defined feature at $76.33 \pm 4.78 \text{ km s}^{-1}$, accompanied by a weaker blueshifted feature at $16.55 \pm 4.61 \text{ km s}^{-1}$. The main $\lambda 1242.804$ line has a similar velocity ($76.91 \pm 4.38 \text{ km s}^{-1}$), but shows only tentative evidence for a blueshifted component.

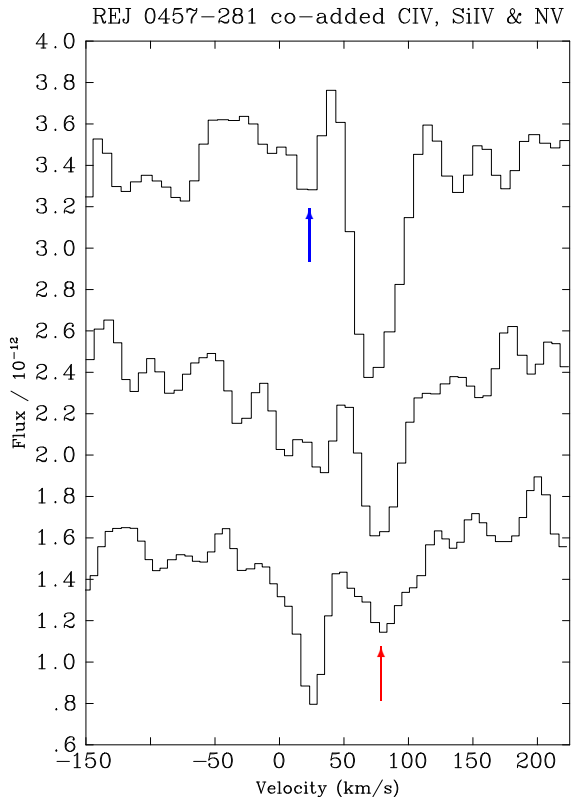


Figure 9. From top to bottom, the co-added lines of the N v, Si iv and C iv doublets in REJ 0457-281. Lower arrow indicates the approximate photospheric velocity, upper arrow shows the position of the shifted components, present in each species.

From these data, a weighted average is computed for the photospheric and blueshifted velocity components, suggesting $v_{\text{phot}} = 76.91 \pm 0.83$, (c.f. 69.60 ± 1.97 from HBS), and $v_{\text{circ}} = 21.76 \pm 1.27$. Thus, the estimated velocity shift of the blueshifted features relative to the photospheric components agrees, within the stated error, with the 53 km s^{-1} value of HBS.

REJ 2156-546

Barstow et al. (1997) determined limits to the heavy element abundance in REJ 2156-546, and described this object as being similar to HZ 43 in having a reasonably pure H atmosphere. The *STIS* spectrum of REJ 2156-546 shows clear interstellar lines, indicating $v_{\text{ISM}} = -8.39 \pm 0.17 \text{ km s}^{-1}$. These new, high resolution data also appear to show features due to photospheric material. The lines are weak, and unambiguous identifications are limited to the strong resonance doublets of SiIV and CIV, although there may be features from NV and NiV at the detection limit. To obtain a reliable value for v_{phot} , the SiIV lines ($\lambda\lambda 1393.755, 1402.777$) were co-added in velocity space, producing a clear feature at $-17.79 \pm 1.33 \text{ km s}^{-1}$, with an equivalent width of $11 \text{ m}\text{\AA}$. Co-addition of the CIV doublet appears to reveal *two* features (figure 10). The first, at $-20.71 \pm 0.80 \text{ km s}^{-1}$, is weak ($4.7 \text{ m}\text{\AA}$), and very close to our value for v_{phot} . The dominant second component lies at $-1.65 \pm 0.76 \text{ km s}^{-1}$, and has an

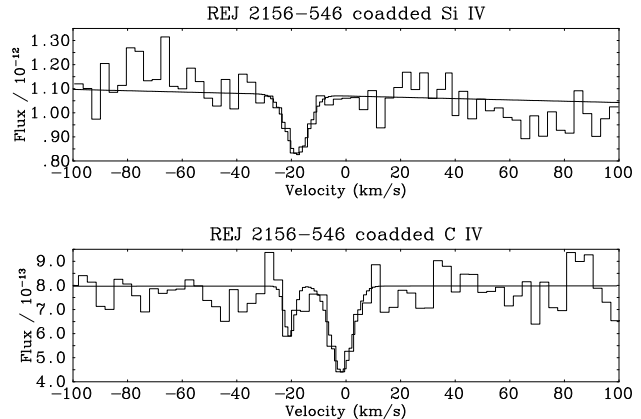


Figure 10. Co-added Si iv and C iv features in REJ 2156-546, with Gaussian fits overlaid.

equivalent width of $20 \text{ m}\text{\AA}$. The weighted average of putative photospheric features produces a value of $v_{\text{phot}} = -19.94 \pm 0.68 \text{ km s}^{-1}$.

The proposed CIV feature lying at a similar velocity to the single SiIV line is admittedly weak, and spectra of improved S/N will be required before these results can be regarded as incontrovertible. Nevertheless, if it is assumed that the object is devoid of any non-photospheric features, whether blue- or redshifted, then the relatively large difference in velocity between the SiIV line and the dominant CIV feature (approximately 16 km s^{-1}) is somewhat difficult to explain. Clearly, this is an object deserving of further attention.

REJ 1614-085

Holberg et al. (1997) found the amount of Si in the spectrum of REJ 1614-085 to be an order of magnitude under-abundant compared to the predictions of radiative levitation calculations, while N appears to be three orders of magnitude over-abundant. Two velocity components were observed in the line of sight ISM, but most significant for the current work is the result that the lines of the CIV and SiIV doublets exhibit weak blueshifted features, as illustrated in figure 11.

Results from this study suggest that the primary ISM component lies at a velocity of $-29.56 \pm 0.33 \text{ km s}^{-1}$, and the secondary component at $+48.64 \pm 1.15 \text{ km s}^{-1}$. These values compare reasonably well with those of Holberg et al., who find velocities of -27.05 ± 1.5 , and $+47.40 \pm 1.50 \text{ km s}^{-1}$ respectively. Similar agreement with the earlier study is also found when considering the photospheric and blueshifted features. The photospheric velocity is found to be $v_{\text{phot}} = -37.31 \pm 0.40 \text{ km s}^{-1}$, in excellent agreement with Holberg et al.. As recorded previously, no clear evidence exists for a secondary component to the photospheric NV lines, although it should be noted that the centroid positions of Gaussian fits to these lines are found to differ by approximately 5 km s^{-1} . In the case of the SiIV doublet, the secondary components are shifted by -40 km s^{-1} relative to the primary features, as determined by Holberg et al. (1997); for the CIV doublet, this figure is -29 km s^{-1} , compared to the value of -25 km s^{-1} quoted by Holberg et al. (1997). This apparent discrepancy is most likely to be a

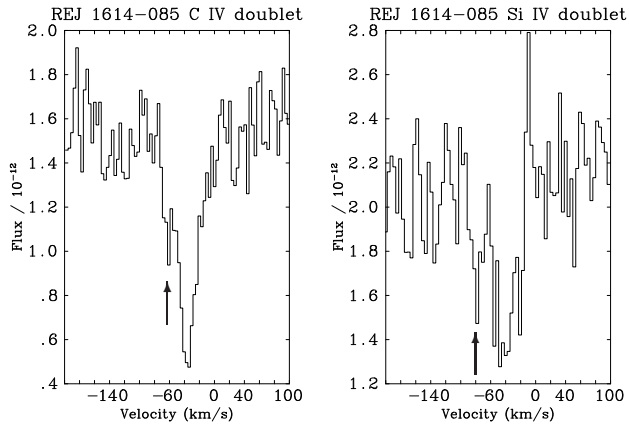


Figure 11. Co-added lines of the C IV (left) and Si IV (right) doublets in REJ 1614-085, in velocity space. The blueshifted components previously noted by Holberg et al. (1997) are indicated by arrows.

result of the different positions chosen for line demarcation in the two studies. A curve of growth analysis performed on the shifted C IV features suggests $N(\text{C IV}) \approx 3.16 \times 10^{13}$ atoms cm^{-2} , and the Doppler parameter $b \approx 2 \text{ km s}^{-1}$, though with only two data points, these values are particularly poorly constrained, and must not be over interpreted.

GD 659

Both *IUE* and *STIS* data are available for this star, although the *STIS* spectrum is of limited coverage (1160 – 1357 Å). The ISM velocity determined from the *IUE* data ($v_{\text{ISM}} = 12.33 \pm 1.52 \text{ km s}^{-1}$) agrees with that of HBS, while the *IUE*-based photospheric velocity appears to be somewhat lower than previously quoted ($v_{\text{phot}} = 33.51 \pm 1.03 \text{ km s}^{-1}$, c.f. $40.31 \pm 1.83 \text{ km s}^{-1}$ from HBS).¹

Since these measurements were made with identical data sets, this discrepancy must be ascribed to differences in choices of continuum levels and line boundaries used during the measurement process. However, the available *STIS* data also point to a lower photospheric velocity, with $v_{\text{phot}} = 34.28 \pm 0.17 \text{ km s}^{-1}$, in agreement with the *IUE* estimate made in this study, and close to the value of 33.58 km s^{-1} determined by Holberg et al. (2000) using *STIS* data. The *STIS* ISM velocity is also lower than the *IUE* value, at $v_{\text{ISM}} = 9.77 \pm 0.22 \text{ km s}^{-1}$. These *STIS* velocities, based on higher resolution data with better S/N, are adopted for GD 659 in table 2. Although the resonance doublets of N V, Si IV and C IV are clearly visible in the *IUE* data, the resolution is insufficient to observe well defined Gaussian profiles, and thus the sensitivity to any non-photospheric components is low. However, the profiles appear to be narrow, ruling out any obvious multiplicity in these lines. *STIS* data show the lines of the N V doublet as narrow and symmetrical, effectively ruling out the existence of non-photospheric N V components.

¹ These features were originally attributed to circumstellar material, and are listed accordingly by HBS, based on the 76 km s^{-1} velocity difference between the UV features and the -37 km s^{-1} Balmer line radial velocity of Wegner (1974). The blueshifted Wegner value is most likely the result of a typographical error.

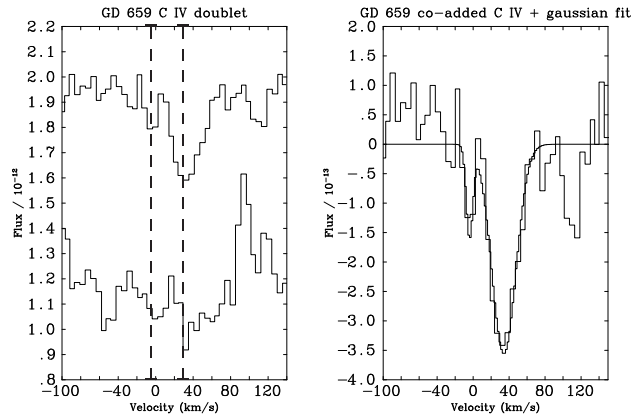


Figure 12. Left: the $\lambda 1548.202$ (top) and $\lambda 1550.774$ (bottom) C IV features in GD 659. Dashed vertical lines indicate the position of a possible secondary component near 0 km s^{-1} , and the primary photospheric line. Flux levels have been adjusted by a constant to allow plotting of features in the same panel. Right: co-addition of the C IV features, with a best-fit double Gaussian profile overlaid.

One interesting feature, clearly visible in the C IV $\lambda 1548.202$ line, though present also in the $\lambda 1550.774$ line, is a weak feature near 0 km s^{-1} (figure 12). Fitting a double Gaussian to the co-added C IV lines, velocities of $36.74 \pm 2.56 \text{ km s}^{-1}$ (primary), and $-2.97 \pm 3.00 \text{ km s}^{-1}$ (secondary) are obtained. The secondary component is weak (with an equivalent width of 6 mÅ compared to 36 mÅ for the photospheric component), and is of comparable strength to scatter in the adjacent continuum regions. Although an *F*-test indicates that a dual Gaussian fit is preferred over a single component at the 94% confidence interval, the similarity between this feature and the natural scatter in the data suggests that this is simply noise. However, until high resolution *STIS* data for this region can rule out the existence of shifted components in the C IV lines, we tentatively include GD 659 among the stars with possible circumstellar features.

2.3.2 Stars with no clear circumstellar features at the resolution of current data

PG 0948+534

PG 0948+534 is the hottest star in this sample. Strong ISM lines are observed, many of which are saturated, and at least two velocity components are present. However, N I and Si II features are most accurately described by three components, with self consistent velocities: the primary component lies at $-0.26 \pm 1.26 \text{ km s}^{-1}$, with the secondary and tertiary components at -22.8 ± 1.2 and $22.1 \pm 2.4 \text{ km s}^{-1}$. These are most clearly revealed by co-addition of the N I and Si II features, as shown in figure 13.

The photospheric lines, including the resonance doublets of C IV and Si IV, exhibit narrow, symmetrical profiles and are apparently devoid of any shifted components, defining $v_{\text{phot}} = -14.25 \pm 0.22 \text{ km s}^{-1}$. A remarkably strong, multi-component C II 1335.7076 Å feature is observed, also shown in figure 13. The velocity components

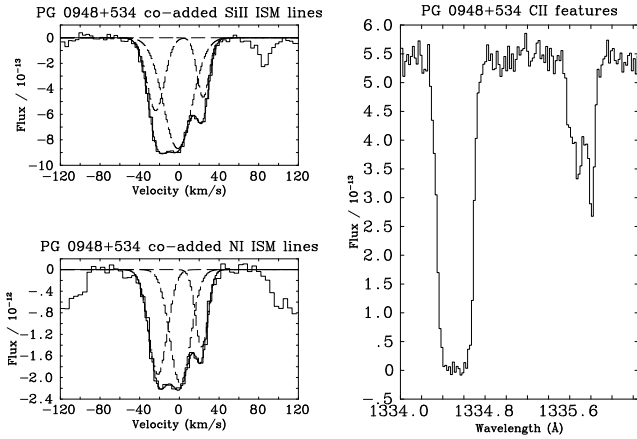


Figure 13. Upper left: co-added interstellar Si II lines in REJ 0948+534, with three-component Gaussian fit. Lower left: analogous plot for N I. Right: interstellar C II lines at $\lambda\lambda 1334.5323, 1335.7076$.

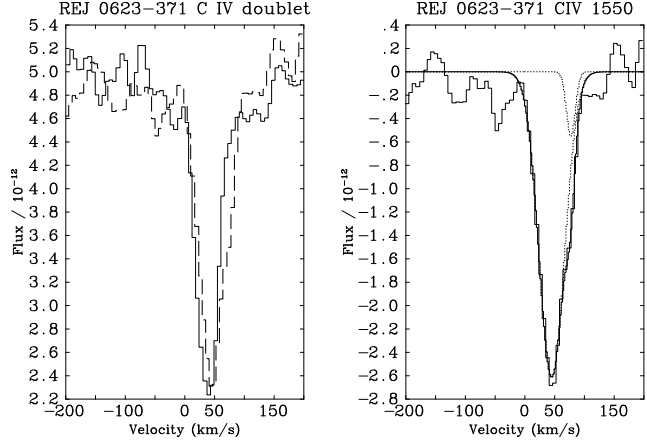


Figure 15. Left: lines of the C IV doublet in REJ 0623-371, in velocity space, demonstrating the difference in velocity of the two lines ($\lambda 1548 =$ solid histogram, $\lambda 1550 =$ dashed histogram). Right: dual Gaussian fit to the 1550 Å C IV line (dashed curves = component Gaussians, solid curve = summed Gaussian).

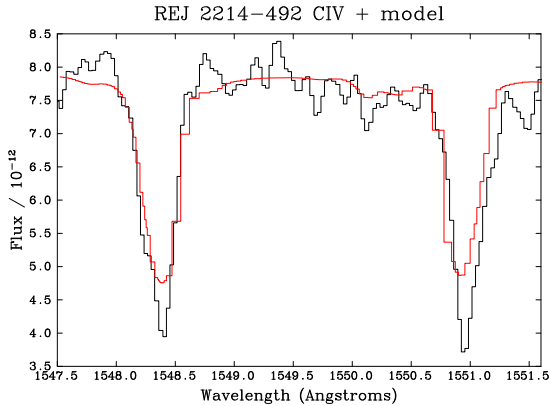


Figure 14. Observed C IV doublet in REJ 2214-492 (black) compared to a synthetic spectrum with $N(\text{C})/N(\text{H}) = 10^{-6}$ $N(\text{H})$, smoothed to the resolution of IUE .

match those of other ISM lines, although the -23 km s^{-1} feature is very weak, manifesting itself as a broadening on the blue side of the line. Excited Si II transitions such as $\lambda\lambda 1265.002, 1309.276, 1533.431$ are not observed (Holberg et al. (1995) used the presence of these lines in the white dwarf CD $-38^\circ 10980$ to infer the existence of a circumstellar cloud around the star). No evidence of highly ionised non-photospheric material is found in PG 0948+534.

REJ 2214-492

Weighted average line velocities indicate $v_{\text{ISM}} = -1.72 \pm 0.51 \text{ km s}^{-1}$, and $v_{\text{phot}} = 33.49 \pm 0.45 \text{ km s}^{-1}$. These values compare well with those of HBS, who find $v_{\text{ISM}} = -0.71 \pm 0.88$ and $v_{\text{phot}} = 33.91 \pm 0.47 \text{ km s}^{-1}$ respectively. However, a significant difference exists between the velocity of each line in the C IV doublet, with $\lambda 1548.202$ at $30.5 \pm 2.1 \text{ km s}^{-1}$, and $\lambda 1550.774$ at $40.4 \pm 2.7 \text{ km s}^{-1}$, if each of the two lines is assumed to be made up of only one absorption feature.

Visual inspection of the C IV doublet reveals slight asymmetry, particularly in the $\lambda 1548.202$ line, where a dual fit was found to be superior to the single Gaussian

at the 99.9% confidence level, with velocity components at 5.37 and 38.36 km s^{-1} , and equivalent widths of 31.1 and 99.3 mÅ respectively. A dual Gaussian fit to the $\lambda 1550.774$ line produced a less obvious improvement (at the 90% confidence level) with components at 36.2 and 80.6 km s^{-1} , and equivalent widths of 137.6 and 14.8 mÅ respectively. The primary Gaussian components of the doublet thus lie at velocities more consistent with each other and the overall photospheric value. The status of putative non-photospheric contributions in the C IV doublet is less certain; although the 5 km s^{-1} feature at 1548 Å appears to provide a good match to observation, the lack of a corresponding feature at 1550 Å prevents confirmation of its reality. No evidence was found for multiplicity in other photospheric lines. Line profiles were compared with those from a model spectrum, produced using the TLUSTY and SYNPEC codes, and adopting the heavy element abundances determined by Barstow et al. (2001) (with $N(\text{C})/N(\text{H}) = 1.0 \times 10^{-6}$). After smoothing the model to the resolution of IUE , no significant differences were apparent in the shapes of model and observed C IV lines (figure 14), casting further doubt on the presence of shifted features in this star.

REJ 0623-371

The photospheric velocity determined here ($v_{\text{phot}} = 41.15 \pm 0.56 \text{ km s}^{-1}$) agrees with that of HBS, though the current value for v_{ISM} is somewhat lower than given by HBS ($16.40 \pm 0.70 \text{ km s}^{-1}$ c.f. $19.48 \pm 0.85 \text{ km s}^{-1}$ respectively); the principal source of this difference lies in a more precise determination of the C II line velocity. HBS estimate the velocity of this line to be $14.07 \pm 3.24 \text{ km s}^{-1}$, compared to the new value of $13.33 \pm 1.14 \text{ km s}^{-1}$.

No compelling evidence exists for the presence of shifted components in the spectrum of REJ 0623-371, but as in the case of REJ 2214-492, a significant difference is observed in the velocity of the lines in the C IV doublet ($1548 \text{ Å} = 38.6 \pm 2.3 \text{ km s}^{-1}$, $1550 \text{ Å} = 47.6 \pm 2.2 \text{ km s}^{-1}$). In contrast, the lines of the NV and Si IV resonance doublets, which are of comparable equivalent width, agree within the

estimated error. Determining the reality of any features in the doublet is complicated by considerable absorption in the continuum of this extremely metal rich DA, though by restricting Gaussian fits to the region below this structure, useful comparisons between the level of agreement found with single and double Gaussian profiles, may be obtained. Using this method, a dual Gaussian fit is preferred to a single feature only at the 88.8% level for the 1548 Å line. However, results for the 1550 Å line are less ambiguous, suggesting a dual fit at 98.9%. The resulting Gaussians have velocities of 45.1 and 77.3 km s⁻¹, and equivalent widths of 128.5 and 10.8 mÅ respectively (figure 15). Thus, while the quality of the available data is insufficient to prove the existence of circumstellar features in the star, the results of this analysis provide some justification for proposing repeat observations at a higher signal-to-noise ratio (S/N) and spectral resolution.

REJ 2334-471

Values measured for v_{ISM} and v_{phot} are in good agreement with those obtained by HBS. The relatively poor quality of the *IUE* data precludes unambiguous identification of any non-photospheric features, particularly in the case of the CIV lines. There is no evidence of multiplicity in the NV doublet, although a dual Gaussian fit to the 1242 Å line, with components at 19.7 and 43.51 km s⁻¹, produces a fit which is preferred over a single feature at the 93% confidence level.

It is therefore intriguing that each line in the SiIV doublet ($\lambda\lambda 1393.755, 1402.777$) is fitted reasonably well (above the 95% confidence interval when compared to a single feature) by double Gaussian profiles. Each line can be described by a double Gaussian with $V_1 = 34.00 \pm 0.82$ km s⁻¹, $EW_1 = 48.85 \pm 0.95$ mÅ, and $V_2 = 54.64 \pm 1.58$ km s⁻¹, $EW_2 = 22.74 \pm 3.25$ mÅ. Neither of the Gaussian velocities are in agreement with the average photospheric value, although a considerable spread in individual photospheric velocity measurements is observed, so that the discrepancy cannot be used to infer the absence of such features. Spectra with improved S/N are required to confirm or disprove the existence of circumstellar features in this star.

GD 246

IUE and *STIS* data were available for this star. Photospheric and ISM line velocities measured from the *IUE* data are in good agreement with those of HBS. The photospheric velocity estimated from *STIS* data differs from the *IUE* value by 1 km s⁻¹, although this is within the *IUE* error bounds. The *STIS* ISM velocity (-5.78 ± 0.12 km s⁻¹) is marginally outside the *IUE* estimate (-7.87 ± 1.00 km s⁻¹). *IUE* and *STIS* data clearly show the CIV doublet lines as singular, and at the photospheric velocity. *STIS* data shows the SiIV $\lambda 1393.755$ line as being devoid of any secondary components, while a sharp feature (only one bin, or 0.02 Å in width) is observed on the redward edge of the $\lambda 1402.777$ line. Although *IUE* data also hint at a broadening on this side of the line, unconvincing dual Gaussian fits, and the extreme narrowness of the extra feature in *STIS* data, suggest that this is due to noise, and thus GD 246 shows no clear evidence of circumstellar material.

PG 1123+189

In the photometric study of hot white dwarfs by Green et al. (2000), this object is one of those listed as having a significant IR excess, suggesting the possibility of a low mass companion to the star.

The *STIS* spectrum for this object is limited in coverage (1163 – 1361 Å), and has relatively low S/N. However, many interstellar lines are visible in the spectrum, and a value of $v_{\text{ISM}} = -0.67 \pm 0.06$ km s⁻¹ is obtained. Although photospheric features are difficult to distinguish in the data, by co-adding the NV lines at 1238 and 1242 Å with those of NiV between 1250 and 1336 Å in velocity space, a single absorption feature is clearly visible, suggesting a value of $v_{\text{phot}} = 12.55 \pm 0.53$ km s⁻¹. The quality of these data is insufficient to confirm or rule out the presence of non-photospheric features with confidence.

HZ 43

A well studied object, HZ 43 is a member of the group of white dwarfs which can be adequately modeled with an atmosphere devoid of any heavy elements. Several ISM lines are observed, leading to an estimate of v_{ISM} which agrees with that of HBS. Co-addition of the spectrum at the wavelengths of the major N, C, Ni and Si lines fails to reveal any photospheric features. Similarly, co-addition, in velocity space, at the wavelengths of the excited Si transitions ($\lambda\lambda 1264.738, 1265.0020, 1309.2758$ and 1533.4312) also shows no new features.

REJ 1032+532

This object is the subject of a comprehensive study by Holberg et al. (1999); Holberg et al. (1999a). In the current work, the measured value of the primary ISM features, $v_{\text{ISM}} = 0.84 \pm 0.21$ km s⁻¹, agrees, within error, with that of Holberg et al. (1999a). A previously noted secondary component to the SiII $\lambda\lambda 1193.2897, 1260.4221$ and 1526.7065 lines is found to have a velocity of -30.43 ± 1.39 km s⁻¹, also in agreement with the value quoted by Holberg et al.. A value of $v_{\text{phot}} = 38.16 \pm 0.40$ km s⁻¹ is determined for the photospheric velocity. The excited SiII lines found around some stars possessing circumstellar clouds (Holberg et al. 1995) are absent, and in none of the photospheric lines is any compelling evidence found for the existence of secondary components.

PG 1057+719

This object (alternative ID REJ 1100+713) is also included in the photometric study of white dwarfs by Green et al. (2000), with no significant IR excess being detected. It belongs to the low opacity metal poor class which includes the majority of DA white dwarfs. Holberg et al. (1997) presented a study of this star and REJ 1614-085 (see below). Their results revealed no signs of circumstellar features.

The current work confirms the results of Holberg et al., revealing no shifted features in the *GHR*S data. Co-addition of the ISM lines results in $v_{\text{ISM}} = -2.89 \pm 0.69$ km s⁻¹. As expected for a low EUV opacity object, no significant photospheric lines are observed. To detect any signs of photospheric features, a series of 10 Å - wide sections were extracted from the data, each centred on the rest wavelength of one of the lines of the NV, CIV and SiIV resonance doublets. The sections were then transformed

into velocity space, and co-added. The presence of barely-detectable quantities of N, C and Si might then be expected to produce a noticeable reduction in continuum level around the photospheric velocity. The co-added data does indeed reveal a feature, with a velocity of 75.35 ± 2.59 km s⁻¹, consistent with the value of $v_{\text{phot}} = 76.1 \pm 3$ km s⁻¹ determined from Balmer line fitting. However, as indicated by Holberg et al., weak individual features found near the expected positions of these lines show a considerable spread in velocity, casting doubt on their authenticity.

GD 394

GD 394 is photometrically variable in the EUV, though no signs of spectroscopic variation have been detected. In contrast to REJ 1614-085, GD 394 has an extreme overabundance of Si compared with model predictions (Holberg et al. 1997). Dupuis et al. (2000) note that this extreme Si abundance, and the observed EUV variability, give a unique status to GD 394. Dupuis et al. present spectroscopic and timing analyses of GD 394, which suggest the presence of a large EUV-dark spot on the surface of the star, sharing the stellar rotation period of 1.150 days. Episodic accretion is proposed as the source of this spot, with a magnetic field directing material onto the magnetic poles. No evidence exists for the presence of a magnetic field in GD 394, though only upper limits can currently be placed on the strength of any such field. GD 394 appears to be an isolated star, and hence no obvious candidate exists for the source of accreted material, other than the immediate stellar neighbourhood.

Early results suggested that the velocity of Si III and Si IV lines differed considerably from the established radial velocity, and that these lines were therefore of a circumstellar origin (Bruhweiler & Kondo 1983). It was also suggested that the absence of any observable Si II features in *IUE* data, which models predicted would be present, represented further evidence for the non-photospheric nature of the heavy elements. However, Barstow et al. (1996) demonstrated that the previous radial velocity measurement, obtained from the Balmer lines, was in error, and a revised value more consistent with the velocities found for the Si features was obtained. By using the latest NLTE models available at the time, Barstow et al. (1996) showed that the predicted abundance of photospheric Si would yield line strengths within the noise of the *IUE* spectrum, and hence the absence of Si II features did not require a non-photospheric solution. Chayer et al. (2000) report the first firm detection of heavy elements other than Si in the spectrum of GD 394, with spectra from the Far Ultraviolet Spectroscopic Explorer (*FUSE*) showing lines of Fe III and P V in the photosphere, as well as a large number of Si III and Si IV lines.

Values of $v_{\text{ISM}} = -7.28 \pm 1.42$ and $v_{\text{phot}} = 28.75 \pm 0.91$ are obtained in this work for the velocity of ISM and photospheric features respectively. As reported by Holberg et al. (1997), the inventory of photospheric lines is dominated by Si III, with additional contributions from the Si IV doublet. Holberg et al. also observe photospheric Al III lines at $\lambda\lambda 1854.7159$ and 1862.7900 . However, C IV and N V are conspicuous only by their absence; co-addition of the data for these wavelengths reveals no trace of features.

No record exists, in recent literature, of circumstellar features in the spectrum. The *IUE* data reveal no sign of C IV or N V, and *GHR*S data are available only for the

ranges 1290 – 1325 Å and 1383 – 1419 Å, which do not include these ions. However, many Si lines are visible in the higher resolution *GHR*S data, and neither individual features or the co-added profiles of all visible Si lines show any form of asymmetry or other qualities which may indicate the presence of circumstellar features. GD 394 is therefore one of the few stars in this survey for which it can be conclusively stated that no shifted features exist, at the resolution of currently available data.

GD 153

Another example of a star which may be modeled with a pure-H atmosphere, GD 153 is a frequently observed standard star. No obvious photospheric features are observed in the *IUE* spectrum of this star, although several ISM lines are recorded, indicating a value of $v_{\text{ISM}} = -8.42 \pm 2.68$ km s⁻¹. This velocity agrees with that obtained by HBS.

EG 102

Holberg et al. (1997) showed that Mg II (λ 4481) and excited Si II was present in the optical spectrum of this cool star. Since radiative levitation calculations predict that much higher temperatures are required before Mg can be suspended in the atmosphere, observable quantities of this species in EG 102 were interpreted as indicative of ongoing accretion, either from a low mass companion (for which no evidence was found) or from a diffuse interstellar cloud. Later, HBS analysed the *IUE* NEWSIPS spectrum of EG 102 and noted the presence of Al III and Al III lines at the photospheric velocity. This observation was also interpreted as being a product of ongoing accretion. Photospheric and ISM velocities determined for EG 102 in this work are in good agreement with those measured by HBS.

Data provided by Chayer et al. (1995) indicate an abundance of $N(\text{Al}) = 10^{-9} N(\text{H})$ for a star with $\log g$ and T_{eff} similar to those of EG 102. The Al abundance in EG 102 has been estimated by fitting data with a pure H model spectrum into which Al has been added, using the code SYNSPEC. After smoothing the output spectrum to the resolution of *IUE*, abundances of order $N(\text{Al}) = 1 \rightarrow 5 \times 10^{-8} N(\text{H})$ are obtained. These figures are significantly higher than those suggested by Chayer et al., but the work of Chayer et al. does not adopt the self-consistent approach found in more recent work (e.g. Dreizler & Schuh (2001); Schuh & Dreizler (2001), discussed in section 1), and a failure to accurately predict the Al abundance in EG 102 cannot be used to infer the presence of accretion processes in the star.

We note that Zuckerman & Reid (1998) find significant quantities of Ca in EG 102² ($\text{Ca}/\text{H} = 2.5 \times 10^{-7}$, $\text{EW} = 29\text{m}\text{\AA}$ for the λ 3933 Ca K line) using high resolution optical echelle spectra obtained with the Keck telescope; current theories of radiative levitation do not predict the Ca ion to be present in such a cool DA. Zuckerman & Reid also find significant quantities of Ca in both of the close white dwarf/red dwarf pairs in their survey, and suggest that the presence of heavy ions such as Ca in cool DA stars may be attributed to binarity. To date, no companion to

² Listed under the alternative name G238-44 in that work.

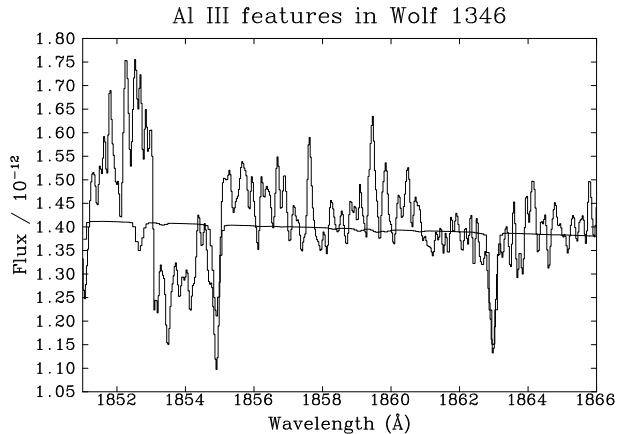


Figure 16. λ 1854, 1862 Å Al III lines in Wolf 1346, with model spectrum superimposed (darker line). The Al abundance inferred from the 1862 Å line is approximately 2.2×10^{-9} N(H). Structure in the continuum level around the λ 1854 line complicated abundance measurements using this feature.

EG 102 has been observed.

Wolf 1346

The presence of Si in the photosphere of Wolf 1346 was revealed by Bruhweiler & Kondo (1982), but later questioned by Vennes et al. (1991), who noted discrepancies between the velocity of Si II lines and the ground-based photospheric velocity, and found that abundances determined from the Si II lines were inconsistent with the non-detection of Si III in the *IUE* spectra of this star – observations more suggestive of a circumstellar origin. The problem was resolved by Holberg et al. (1996), who revised the photospheric velocity and used the advanced non-LTE code TLUSTY to derive a Si abundance 0.5 dex lower than that of Vennes et al., confirming the photospheric nature of the Si lines.

The velocities of features normally associated with the ISM appear to fall into two groups, at -16.19 ± 0.10 km s $^{-1}$ and -7.67 ± 3.07 km s $^{-1}$. When considering the velocities of *isolated* features, these groups appear to contain separate species (OI, C II and S II at -16 km s $^{-1}$, and Si II at -7 km s $^{-1}$). However, this segregation breaks down when those interstellar Si II features which are blended with photospheric features, are included. For example, the ISM component of the λ 1260.4221 Si II line, lies at -16.73 km s $^{-1}$.

The photospheric lines (which are limited to Si II and Si III) show a considerable spread in velocity (from 19 to 33 km s $^{-1}$), with the weighted mean being $v_{\text{phot}} = 24.32 \pm 1.41$ km s $^{-1}$. Given this range of velocities, the reality of the two ISM groupings is questionable. Data from HBS also show this grouping, though only four ISM lines are recorded (compared to ten in the current study). HBS treat these velocities as belonging to the same group, and give a weighted mean ISM velocity of -14.85 ± 1.50 km s $^{-1}$. For the current work, the analogous value is $v_{\text{ISM}} = -15.38 \pm 0.95$ km s $^{-1}$. Thus, both v_{ISM} and v_{phot} are found to agree with the values presented by HBS.

Lines of Al III are clearly visible at the photospheric velocity. These features are not noted in previous studies of Wolf 1346 (Holberg et al. (1996), HBS). To estimate the Al abundance, the λ 1854, 1862 lines were reproduced by

Star	Species
REJ 1738+665	C IV , Si IV , NV, OV.
Ton 021	C IV , Si IV.
REJ 0558-373	C IV .
WD 2218+706	C IV , Si IV .
Feige 24	C IV .
G191-B2B	C IV , Si IV *.
REJ 0457-281	C IV , Si IV , NV.
REJ 2156-546	C IV.
REJ 1614-085	C IV , Si IV .
GD 659	C IV.

* Detected by Holberg et al. (2002).

Table 3. Ionic species contributing to observed or suspected circumstellar features. Ions responsible for principal features (i.e. those which are clearly identifiable without the need for co-addition) are indicated in bold; other species should be regarded as tentative identifications.

adding quantities of Al to a spectrum generated from a pure H+He non-LTE model ($N(\text{He}) = 10^{-8}$ N(H)), and the output smoothed to the resolution of *IUE* (~ 0.2 Å FWHM). An abundance of $N(\text{Al}) = 2.2 \times 10^{-9}$ N(H) was found to match the observed 1862 Å line, and is close to the value of $\sim 1 \times 10^{-9}$ N(H) implied by the results of Chayer et al.. A greater abundance ($N(\text{Al}) = 6.0 \times 10^{-9}$ N(H)) was required to match the 1854 Å feature; however, the region around this line exhibits unusual structure, possibly due to instrumental effects. The models used to determine these abundances are *not* stratified, and hence these values are likely to be revised when suitable stratified models become available. The Al lines and synthetic spectrum are illustrated in figure 16.

3 DISCUSSION

Of the twenty three stars considered in this survey, four were previously known to possess features from highly ionised species at non-photospheric velocities: Feige 24, REJ 0457-281, G191-B2B and REJ 1614-085. Four new DA white dwarfs may now be added to the list of those exhibiting unambiguous, highly ionised components at non-photospheric velocities: REJ 1738+665, Ton 021, REJ 0558-373, and WD 2218+706. A fifth object, REJ 2156-546, shows features which may also be interpreted as non-photospheric, although data of improved S/N are required to confirm this result. A weak blueshifted component in GD 659 is also suggested, though this is exceedingly faint, comparable with the structure of adjacent noise, and hence regarded as a tenuous identification until further data become available. Table 3 lists those ions appearing as circumstellar features. Observations of these features are restricted to resonance transitions, and are most common in the C IV $\lambda\lambda$ 1548.202, 1550.774 doublet (the resonance lines are most strongly coupled to the stellar radiation field, and hence are more susceptible to radiative levitation). The velocities of interstellar, photospheric and non-photospheric features (if detected) have been presented in table 2.

Of the eleven *IUE* spectra considered in this study, only one (REJ 0457-281) shows signs of highly ionised, non-photospheric components. In contrast, six out of the twelve

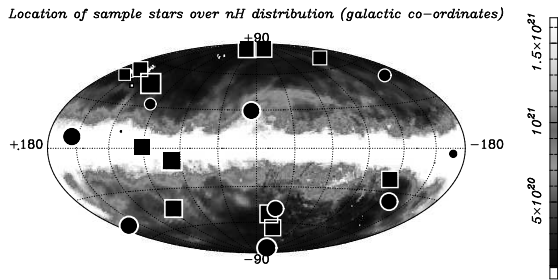


Figure 17. The distribution of survey stars in galactic coordinates. Circles indicate stars in which circumstellar features are observed, with all other objects plotted as squares. Symbol size indicates distance (larger = closer). Objects are plotted over the galactic H I map of Dickey & Lockman (1990) (units are cm^{-2}).

available *STIS* spectra reveal such features (with a further detection in one of the three available *GHRIS* spectra). The low number of detections in *IUE* data is unsurprising given the low signal-to-noise ratio of the instrument, and the fact that its resolution (0.08 \AA at 1400 \AA) is equivalent to a velocity of 17 km s^{-1} (compared to $\sim 3.2 \text{ km s}^{-1}$ with the *STIS* E140M grating, and $\sim 1.28 \text{ km s}^{-1}$ in the E140H configuration). The non-detection of circumstellar components in *IUE* data therefore places an upper limit on the velocity of any shifted features, rather than proving absence. *STIS* data may yet reveal non-photospheric features in these objects.

The need for consistently high resolution data with adequate S/N, covering *all* stars in follow-up studies is clear. Only the highest resolution *STIS* data were able to show secondary features in the ISM lines of G191-B2B, revealing a possible connection between the circumstellar components and the local ISM. These features were not resolved in the *STIS* E140M data. However, all but one of the *STIS* spectra included in this survey were acquired with the E140M grating (PG1123+189 was observed in the higher resolution E140H mode, but the data do not cover the C IV or Si IV resonance lines). Hence, more stars in the current sample may possess highly ionised non-photospheric features, at velocity differentials too small for the existing data to resolve. Alternatively, some stars may possess very weak circumstellar features which are hidden within the noise of existing data. Only when *STIS* data (ideally from the E140H configuration and covering the important resonance lines) are available for all stars in this sample, will a more comprehensive study of the distribution of circumstellar features in white dwarfs be possible.

3.1 Influence of position and intervening ISM column

3.1.1 Spatial distribution

The distribution of survey stars is depicted in figure 17; no correlation between the presence of circumstellar features and the position of objects on the sky is apparent. Since the sample stars encompass a relatively wide range of distances (between approximately 14 and 436 pc), the absence of such a positional dependence is not surprising.

3.1.2 ISM $N(\text{HI})$ column density

Line-of-sight ISM $N(\text{HI})$ column densities may be estimated by fitting models to the observed ISM Ly- α profile (after removing the stellar contribution to line+continuum using a stellar model), as demonstrated by Barstow et al. (1994a) and Holberg et al. (1999a). Alternatively, the HI column density may be determined from *EUVE* data using the strong continuum absorption below the 912 \AA Lyman edge. In this case, the column density is included as a free parameter in model spectra, which are fitted to the data using χ^2 reduction techniques (e.g. Barstow et al. 1999; Holberg et al. 1999a). These methods provide the *average* column density, and are insensitive to “clumping” along the line of sight. As an extension to this simplification, it may be assumed that, *ceteris paribus*, a more distant star along the same or similar line of sight will be observed through an intervening column, $N(\text{HI})$, of greater density. The figure of interest is therefore the volume density $n(\text{HI})$ along the ISM column, where, in the general case,

$$N(\text{HI}) = \int_0^s n(\text{HI}) ds, \quad (1)$$

and where s is the distance to the star. For a homogeneous column, $n(\text{HI}) \approx N(\text{HI})/s$.

Previously determined column densities are available for many of the sample stars, while approximations may be made for others using the synthesis maps of Frisch & York (1983), and the contour maps of Paresce (1984). These columns are listed in table 4, showing that a relationship between circumstellar features, and the average density of interstellar material along the line of sight, is not observed. For example, both REJ 1738+665 and REJ 0457-281 show circumstellar features, yet their line of sight ISM volume densities are significantly lower than objects without such features.

This result is not surprising. Dupree & Raymond (1983) find that for a DA white dwarf with $T_{\text{eff}} = 60,000\text{K}$ and $\log g = 8.0$, the Strömgren radius ranges from 0.07 pc (for $n(\text{H})=10^2 \text{ cm}^{-3}$) to 30.8 pc ($n(\text{H})=0.01 \text{ cm}^{-3}$). Although their work is now dated (the heavy element features in white dwarf spectra are attributed to the ionisation of circumstellar material), these figures still provide a useful order of magnitude estimate for the sphere of influence of the white dwarf. It could also be argued that the quoted Strömgren radii represent upper limits, since the extra opacity from photospheric heavy elements would be expected to reduce the intensity of the radiation field at specific wavelengths. In either case, the Strömgren radius is typically a small fraction of the distance to the star, and since the distribution of material along the line of sight is unlikely to be homogeneous, the observed average value of $n(\text{HI})$ may not reflect conditions within the Strömgren sphere.

3.1.3 The velocity of circumstellar features and the ISM

For a white dwarf which is ionising nearby interstellar material, highly ionised non-photospheric components may be observed at velocities similar to those of the intervening ISM. Depending on the relative velocities of star and ISM, this mechanism will produce both red- and blue-shifted features.

The majority of stars possessing circumstellar compo-

Table 4. H I column and volume densities for the survey stars, obtained from a variety of previous studies. Data from Frisch & York (1983) and Paresce (1984) should be interpreted as broad estimations only. No data available for REJ 0948+534 or EG 102.

Star	N(HI) (cm ⁻²)	n(HI) (cm ⁻³)	Reference
REJ 1738+665 ^{a,*}	< 5.0 × 10 ¹⁸	< 6.7 × 10 ⁻³	Barstow et al. (1994b)
Ton 021*	1 → 5 × 10 ²⁰	1.5 → 7.5 × 10 ⁻¹	Frisch & York (1983)
REJ 0558-373*	1 → 5 × 10 ²⁰	1.1 → 5.5 × 10 ⁻¹	Frisch & York (1983)
REJ 2214-492	5.8 × 10 ¹⁸	2.73 × 10 ⁻²	Wolff et al. (1998)
REJ 0623-371	5.0 × 10 ¹⁸	1.67 × 10 ⁻²	Wolff et al. (1998)
WD 2218+706*	> 10 ²¹	> 7.4 × 10 ⁻¹	Frisch & York (1983)
Feige 24*	3.25 × 10 ¹⁸	1.35 × 10 ⁻²	Wolff et al. (1998)
REJ 2334-471	8.5 × 10 ¹⁸	2.65 × 10 ⁻²	Wolff et al. (1998)
G191-B2B*	2.1 ± 0.1 × 10 ¹⁸	1.4 × 10 ⁻²	Barstow et al. (1999)
GD 246	> 1.51 × 10 ¹⁸	> 6.8 × 10 ⁻³	Fruscione, A. et al. (1994)
REJ 0457-281*	(1.3 ± 0.7) × 10 ¹⁷	3.9 × 10 ⁻⁴	Barstow et al. (1994a)
PG 1123+189	1.10 × 10 ¹⁹	2.4 × 10 ⁻²	Holberg et al. (1999b)
HZ 43	9.3 ± 0.1 × 10 ¹⁷	4.2 × 10 ⁻³	Barstow et al. (1995)
REJ 1032+532	4.2 × 10 ¹⁸	1.1 × 10 ⁻²	Holberg et al. (1999b)
REJ 2156-546*	4.1 × 10 ¹⁸	1.0 × 10 ⁻²	Holberg et al. (1999b)
PG 1057+719	2.75 × 10 ¹⁹	2.17 × 10 ⁻²	Wolff et al. (1998)
REJ 1614-085 ^{a,*}	≈ 5 × 10 ²⁰	≈ 1.89	Paresce (1984)
GD 394	4.4 × 10 ¹⁸	2.5 × 10 ⁻²	Barstow et al. (1996)
GD 153	6.03 × 10 ¹⁷	2.68 × 10 ⁻³	Fruscione, A. et al. (1994)
GD 659*	3.2 × 10 ¹⁸	2.0 × 10 ⁻²	Holberg et al. (1999b)
Wolf 1346	1.10 × 10 ¹⁸	2.55 × 10 ⁻²	Fruscione, A. et al. (1994)

*Circumstellar features observed or suggested.
^aTotal column (N_H) quoted

nents show little agreement between v_{circ} and v_{ISM} . This result is unsurprising, since observed ISM absorption features may be blends of several unresolved ISM components at the resolution of the current data, and hence the dominant component (typically the LISM) may not be that in which the star is immersed. Nevertheless, it is useful to consider the residual value of $|v_{\text{ISM}} - v_{\text{circ}}|$ (figure 18). These data show that in the majority of objects possessing circumstellar features, the difference in velocity between these and the primary interstellar cloud is typically 10 km s⁻¹ or less (exceptions being REJ 1614-085 and GD 659). The most interesting cases are found in REJ 1738+665 and G191-B2B, where excellent agreement is found between v_{ISM} and v_{circ} , suggesting that the shifted features arise in a Strömgren sphere of material belonging to the primary identified ISM component.

More detailed investigations are required before this hypothesis can be confirmed, and a detailed analysis of the ion populations and spectral characteristics of such a system is essential. The case of G191-B2B also acts as a caution against over-interpretation of these results; no correlation between v_{ISM} and v_{circ} would have been recognised if not for the higher resolution data discussed by Sahu et al. (1999). Similar correlations with hitherto undetected ISM components may be found in future studies based on E140H grating spectra. Despite the relatively narrow wavelength coverage available with this instrument, the current results justify a comprehensive program of E140H white dwarf observations, possibly tuned to a bandpass covering the CIV resonance doublet, which is most frequently accompanied by shifted features.

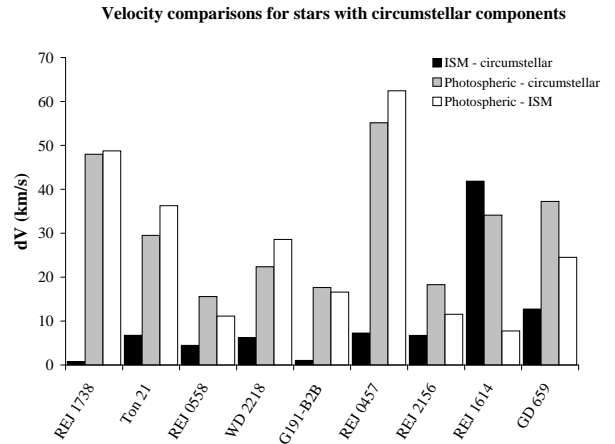


Figure 18. Comparison between photospheric, ISM and circumstellar velocities in stars showing highly ionised non-photospheric features (Feige 24 omitted since v_{circ} and v_{phot} vary with orbital position, while v_{ISM} is stationary).

3.2 Metallicity and mass loss

MacDonald (1992) discusses the interaction between the flow of ISM material around a white dwarf star, and the weak stellar wind. In this work, the rate of mass loss, \dot{M} , from the white dwarf is estimated using theory developed by Abbott (1982), viz.

$$\dot{M} \approx 2 \times 10^{-15} \left(\frac{L}{L_{\odot}} \right)^2 \frac{Z}{0.02} M_{\odot} \text{ yr}^{-1}, \quad (2)$$

where Z is the metallicity, relative to solar abundances, of a star with luminosity L and mass M .

However, the work of Abbott is concerned with the envelopes of O- to G-type stars, and results are found to be most successful for OB stars. Conversely, the theory does not explain mass loss rates in Wolf-Rayet stars, which are somewhat different in structure. Further, since the theory of Abbott is concerned with main sequence objects, the metallicity parameter is formulated in terms of solar abundances, and cannot be applied directly to the broad range of heavy element compositions exhibited in white dwarfs. Hence the use of equation 2 in the current work is not entirely appropriate.

Nevertheless, it is interesting to compare the *relative* mass loss rates of sample objects calculated using equation 2. Individual abundances have been calculated by Barstow et al. (2001). These values were determined by matching observational data to a synthetic spectrum calculated using SYNSPEC, based on a model of appropriate T_{eff} and $\log g$ generated by the non-LTE code TLUSTY. This information is available for all objects in the sample except PG 0948+534 (table 5). For each star, the metallicity parameter, Z , is calculated using the expression

$$Z = \left(\sum_{z>2} A_*(z) \right) \left(\sum_{z>2} A_{\odot}(z) \right)^{-1}, \quad (3)$$

where $A_{*,\odot}$ is the abundance of the element of atomic number z relative to hydrogen in the star and in the Sun³ respectively. Only “metals” (elements heavier than He) are included. Note that although equation 3 should be evaluated for all elements heavier than He, only clearly identifiable species as presented in table 5, have been considered here.

Stellar luminosities quoted in table 5 have been calculated from the familiar expression

$$L_* = 10^{0.4\{M_{\odot} - M_*\}} L_{\odot}, \quad (4)$$

where M_{\odot} represents the absolute bolometric magnitude of the Sun (+4.7), or the star (calculated using the stellar models of Wood 1995).

No clear correlation is found between \dot{M} and the presence of circumstellar features, although loss rates extend to lower values for objects without these features (figure 19). The lowest values are found in the coolest stars, as expected given the dependence of equation 2 on luminosity and metallicity. However, GD 246 ($T_{\text{eff}} = 53,700\text{K}$) is significantly hotter than REJ 1614-085 ($T_{\text{eff}} = 38,500\text{K}$) despite having an appreciably lower calculated loss rate. While the subset of stars which exhibit non-photospheric components lacks any object with $\dot{M} < 3 \times 10^{-15} M_{\odot} \text{ yr}^{-1}$, (compared to a minimum value of $1.9 \times 10^{-21} M_{\odot} \text{ yr}^{-1}$ for those with no circumstellar components), the number of objects in this survey is insufficient to determine the authenticity of a lower limit to the mass loss rates in stars showing highly ionised, non-photospheric components.

³ Using data provided by Grevesse & Sauval (1998), $\sum_z A(z)_{\odot} \approx 1.18\text{E-}3$, where $z=6, 7, 8, 14, 15, 16, 26$ and 28, reflecting the elements considered in table 5.

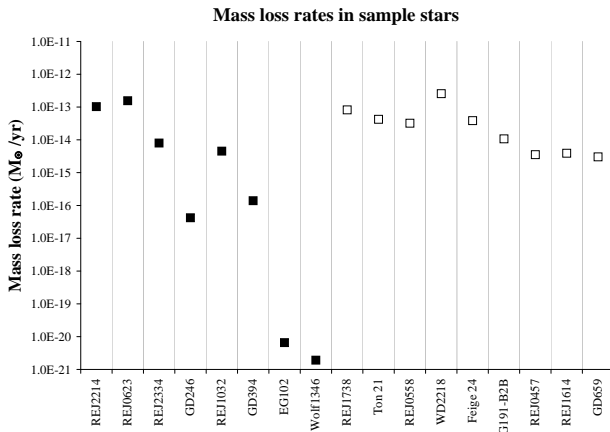


Figure 19. Calculated mass loss rates for those sample stars containing metals, as defined in table 5. *Filled squares*: stars with no observed circumstellar features. *Open squares*: stars exhibiting circumstellar features. Objects for which no metals are present or for which data are unavailable have been omitted.

3.3 Gravitational Redshift

The apparent velocity of absorption features formed in the white dwarf atmosphere will be affected by the radial velocity of the star, and by gravitational redshifting. The velocity change due to gravitation will be lower in features which are formed in material further from the stellar surface (e.g. a circumstellar cloud), and will be effectively zero for a cloud with a sufficiently large inner radius. The gravitational redshift at the stellar surface therefore defines a range of velocities, with respect to the apparent photospheric value, at which highly ionised non-photospheric features *may* be attributed to material residing within the gravitational well of the star.

Gravitational redshifts can be measured directly in binary systems such as Feige 24 (Dupree & Raymond 1982; Vennes & Thorstensen 1994), but for isolated systems, the velocity component due to gravitation redshift, v_{grav} , can be estimated using the standard formula,

$$\frac{\lambda_{\text{obs}} - \lambda_{\text{rest}}}{\lambda_{\text{rest}}} = \frac{v_{\text{grav}}}{c} = \frac{GM}{c^2 R}, \quad (5)$$

where G is the universal constant of gravitation, M is the stellar mass, R is the radius (of the star, or of the circumstellar cloud), c is the speed of light, and $\lambda_{\text{obs,rest}}$ are the observed and rest wavelengths of the absorption line, respectively. Substituting values for the physical constants, the expression for v_{grav} becomes simply

$$v_{\text{grav}} \approx 6.36 \times 10^2 \frac{M_*}{R_*} \text{ m s}^{-1}, \quad (6)$$

where solar units are to be used for the white dwarf mass and radius. In the work which follows, estimates using this expression are used to identify features which could arise from material residing well within the gravitational potential of an object.

Values for v_{grav} , calculated using equation 6, are included in table 2. The presence of material in the gravitational potential well of a star provides no explanation for objects in which material appears at a velocity redshifted with respect to the photospheric value, as in the case of WD

Table 5. Photospheric heavy element abundances of the surveyed stars, determined from far-UV spectroscopy (no data available for PG 0948+534). Note that gaps in the table for those stars up to (and including) REJ 0457-281 are mostly due to the absence of data for a particular spectral range rather than a true absence of the element itself. For the remaining, cooler stars, gaps in the table reflect genuine absence of these species at abundances detectable by *IUE* or *STIS*. From Barstow et al. (2001).

Star	C/H	N/H	O/H	Si/H	P/H	S/H	Fe/H	Ni/H	Z	L	\dot{M}
REJ 1738+665*	2.0E-8	3.0E-7	3.0E-7	1.0E-6			4.0E-6	5.0E-7	5.18E-3	12.59	8.21E-14
Ton 021*	5.4E-7	8.4E-8	1.2E-7	2.7E-6			1.3E-6	6.6E-8	4.07E-3	10.19	4.22E-14
REJ 0558-373*	8.0E-7	3.0E-7	3.0E-6	2.0E-6	2.0E-8	2.5E-7	1.0E-5	1.5E-6	1.51E-2	4.61	3.22E-14
REJ 2214-492	1.0E-6	7.5E-8	9.6E-7	7.5E-7			1.0E-5	1.0E-6	1.17E-2	9.38	1.03E-13
REJ 0623-371	1.0E-6	1.6E-7	9.6E-7	3.0E-7			1.0E-5	1.0E-6	1.14E-2	11.69	1.55E-13
WD 2218+706*	4.0E-7	1.0E-6	1.0E-5	6.5E-7			2.0E-5	5.0E-7	2.76E-2	9.64	2.56E-13
Feige 24*	1.0E-7	3.0E-7	5.0E-7	3.0E-7			1.0E-5	2.0E-6	1.12E-2	5.86	3.84E-14
REJ 2334-471	2.0E-8	5.0E-7		3.0E-7			1.0E-5	5.0E-7	9.59E-3	2.88	7.97E-15
G191-B2B*	4.0E-7	1.6E-7	9.6E-7	3.0E-7	2.5E-8	3.2E-7	1.0E-5	5.0E-7	1.07E-2	3.16	1.07E-14
GD 246				1.0E-7					8.47E-5	2.23	4.21E-17
REJ 0457-281*	4.0E-7	1.6E-7	9.6E-7	1.0E-7	2.5E-8		1.0E-5	5.0E-7	1.03E-2	1.85	3.53E-15
PG 1123+189									—	2.75	—
HZ 43									—	1.49	—
REJ 1032+532	4.6E-7	5.0E-5		5.6E-8					4.28E-2	1.03	4.52E-15
REJ 2156-546*									—	1.06	—
PG 1057+719									—	0.64	—
REJ 1614-085*	4.8E-7	2.5E-4		1.0E-8					2.12E-1	0.43	3.90E-15
GD 394				8.0E-6					6.77E-3	0.45	1.39E-16
GD 153									—	0.56	—
GD 659*	2.0E-7	6.3E-4		1.6E-8					5.34E-1	0.24	3.01E-15
EG 102				1.0E-7					8.47E-5	0.03	6.54E-21
Wolf 1346				3.2E-8					2.71E-5	0.03	1.91E-21

*Circumstellar features observed

2218+706, Feige 24, REJ 2156-546, and REJ 1614-085. The mechanism may also be ruled out for three further stars, REJ 1738+665, Ton 021 and REJ 0457-281, in which the calculated gravitational redshift is substantially lower than required to explain the velocity of non-photospheric components.

For the three remaining stars, the gravitational redshift is comparable to the velocity difference between photospheric and circumstellar components. However, if the calculated values of v_{grav} are assumed to be reasonable, only circumstellar features in REJ 0558-373 may be explained by the presence of matter inside the gravitational well (at approximately 5 stellar radii from the surface). In the cases of G191-B2B and GD 659, the non-photospheric components differ from v_{phot} by an amount equal to, or slightly greater than, the value of v_{grav} . This suggests that the material lies at a radius greater than that at which gravitational redshifting produces observable changes in line velocity. It is therefore apparent that, with the possible exception of REJ 0558-373, blueshifted features in the spectra of objects in this study cannot be explained by the presence of material within the gravitational potential well of the star.

3.4 Non-photospheric material and its relation to planetary nebulae

The existence of an old planetary nebula (PN) around two of the survey stars has already been addressed in the cases of REJ 1738+665 and WD 2218+706. Mass loss and the production of a PN as a white dwarf progenitor leaves the AGB, are relatively well accepted processes (though the precise details are certainly not (Langill et al. 1994)). It is therefore

pertinent to ask whether the presence of non-photospheric, highly ionised features around other DA stars at the hotter end of the sample (i.e. those for which the nebula material may not be completely dispersed), is consistent with material from a (now ancient) PN around the star.

Expansion velocities for PNe are available in the literature (e.g. Weinberger 1989). The study by Napiwotzki & Schönberner (1995) is particularly relevant, since it deals specifically with old planetaries, with central stars in the advanced stages of transition into the white dwarf area of the H-R diagram. Since even the hottest stars in the current study are more highly evolved than those covered by Napiwotzki & Schönberner, average temperatures are cooler, and any nebular material presumably of lower density and more widely dispersed. Direct detection of nebular emission around these stars is therefore difficult, excepting the two cases previously highlighted. Further, in the case of the older, cooler stars in the current work (e.g. REJ 2156-546 and REJ 1614-085), the planetary nebula must have dispersed long ago, and is therefore unlikely to offer an explanation for the existence of highly ionised, non-photospheric features. Nevertheless, the possibility that some circumstellar features are of this origin may be assessed by comparison with the expansion velocities noted by Napiwotzki & Schönberner.

Figure 20 shows the distribution of expansion velocity (in this case plotted against nebula radius) for the objects investigated by Napiwotzki & Schönberner. No data are available for the radius of any PNe which may surround stars in the current survey; however, an analogous velocity can be derived in the form of the difference between the velocity of circumstellar and photospheric features, as listed in

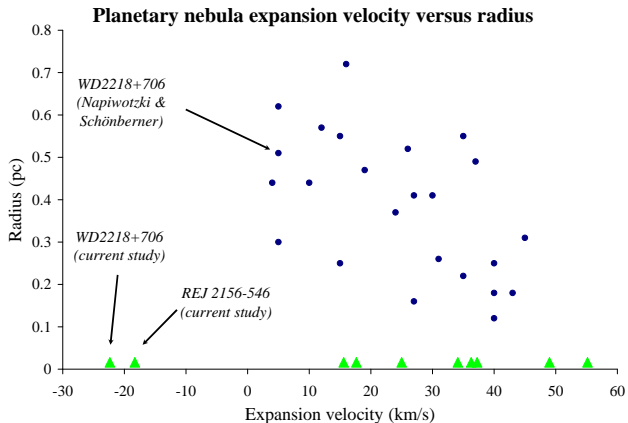


Figure 20. Circles: Nebula expansion velocity v_{exp} plotted against nebula radius, for stars studied by Napiwotzki & Schönberner (1995). Triangles: $v_{phot} - v_{circ}$ for stars in the current work (no values for radius are available).

table 2. Note that WD 2218+706 (DeHt5) is common to both studies, and in this case the true value of v_{exp} , as determined by Napiwotzki & Schönberner, is considerably different to the *negative* velocity, relative to the photospheric value, found in the current work. It is therefore clear that the non-photospheric features of WD 2218+706 discussed in the current study are not produced by the observed planetary nebula (though the nebula cannot be discounted as a *source* of this material).

We note that the observation of features which are redshifted with respect to the photosphere is not incompatible with the nebula hypothesis; for example, Tweedy & Napiwotzki (1994) discuss the planetary nebula Sh 2-174 and the white dwarf GD 561 observed on one edge of this nebula. The objects are found at similar distances, and [O III] emission in the nebula is located immediately adjacent to the white dwarf. These observations, the statistical improbability of GD 561 being an isolated hot white dwarf which happens to be wandering through the nebula, and the difficulty in explaining the existence of a small nebula other than being of PN origin, confirm that GD 561 is indeed the source of the planetary nebula. The distinctly non-spherical morphology of Sh 2-174 is far from unique in studies of old PNe (Tweedy & Napiwotzki and references therein). Gross asymmetries are attributed to interaction between the nebular material and the surrounding ISM through which it moves. Given the location of GD 561 relative to the central region of Sh 2-174, it is clear that the PN material may produce spectral features which are either blue- or red-shifted with respect to the photosphere, depending on the angle from which the system is viewed.

For all but two of the stars in this work, $v_{phot} - v_{circ}$ is of a similar order of magnitude as the expansion velocity typical of old PNe. Two stars (WD 2218+706 and REJ 2156-546) are shown with the negative values of v_{circ} discussed above - but the absolute values, $|v_{phot} - v_{circ}|$, are consistent with the remainder of the sample. In contrast, radiatively driven winds from the surface of a white dwarf should be of a similar order to the stellar escape velocity, i.e. $\sim 1000 \text{ km s}^{-1}$ or more (MacDonald 1992). These results may indicate some form of link between the origin of the non-photospheric

absorbing matter, and the old, dispersed PN material surrounding these stars.

The results of this comparison suggest that further work on the link between highly ionised non-photospheric features, and planetary nebulae is justified. Although this hypothesis appears to contradict the suggestion that shifted features may be related to interstellar material within the Strömgren sphere of a white dwarf, *both* mechanisms may operate in different objects, with Strömgren spheres as the dominant source for cooler objects. Correlating typical PNe densities with the column densities derived from curve of growth analysis would provide further evidence of a relationship between these two apparently separate entities. This comparison is complicated by the considerable difficulty in estimating the masses of PNe, arising from uncertainties in the distances to nebulae, and from the ongoing debate as to whether these objects are typically ionisation or mass bounded.

4 SUMMARY

We have described the detection and interpretation of highly ionised absorption features at non-photospheric velocities, in high resolution UV spectra of hot DA white dwarfs. These features may be indicative of accretion or mass loss in white dwarfs – processes which may explain the non-equilibrium abundances, compared with the predictions of radiative levitation theory, observed in many objects. Four of the stars in the sample were previously known to show non-photospheric features: Feige 24, REJ 0457-281, G191-B2B and REJ 1614-085. This work has revealed at least four new objects with multiple components in one or more of the principal resonance lines: REJ 1738+665, Ton 021, REJ 0558-373 and WD 2218+706. A fifth object, REJ 2156-546 also shows some evidence of multiple components, though further observations will be required for their reality to be confirmed.

Several possible mechanisms for the formation of these features have been discussed. The presence of material within the gravitational potential well of a white dwarf is found to be an unsatisfactory explanation for the production of these features. Predicted mass loss rates based on the luminosity and metallicity of stars show no correlation with the presence of shifted features. However, these mass loss rates are calculated using theories developed for main sequence stars, and may be inappropriate for application to highly evolved objects. Further, the quantification of metallicity is a highly subjective measurement, and is likely to be a major source of uncertainty in these calculations.

A possible correlation is observed between the velocity of shifted features and that of the ISM. This is particularly obvious in REJ 1738+665 and G191-B2B, which show very close matches between v_{ISM} and v_{circ} . For most of the remaining stars, the difference between these velocities is less than 10 km s^{-1} . Higher resolution observations are required to detect the presence of multiple ISM velocity components, which may reveal further correlations – as demonstrated by the case of G191-B2B.

An alternative or additional source of shifted features may be found in planetary nebulae. Velocities of shifted features with respect to the photosphere in this study are found to be entirely consistent with the expansion velocities typ-

ical of old PNe. By appealing to the irregular morphology of highly evolved nebulae, both blueshifted and redshifted features may be explained. Detailed modeling of the interaction between the white dwarf and surrounding material should determine whether stellar radiation alone is sufficient to produce the observed ionisation, or whether additional excitation (perhaps in the form of shock-heating) is required (Napiwotzki, private communication).

The non-detection of highly ionised non-photospheric features in many of the stars investigated may indicate their absence, but equally, may reflect the limited resolution and signal-to-noise ratio of available data. This is particularly important when considering non-detections in *IUE* data, where velocity differentials of less than 17 km s^{-1} between photospheric and shifted components are below the resolution limit of the instrument, and where the S/N ratio is inferior to that of more modern instruments such as *STIS*. This highlights the importance of acquiring consistently high resolution data for all stars in this and future samples. Four (and possibly five) new identifications of circumstellar features have been made using medium resolution (E140M) *STIS* spectra; these successes demonstrate the value in high resolution studies of this type, and justify an extension of the program to include higher resolution data of improved S/N for an expanded sample of objects.

5 ACKNOWLEDGEMENTS

NPB and MAB were supported by PPARC. JBH wishes to acknowledge support of for this work provided by NASA through grant GO-7296 and AR-9202 from the Space Telescope Science Institute, which is operated by the Association of Universities for Research in Astronomy, incorporated under NASA contract NAS 5-26555. We thank Cherie Miskey (Institute for Astrophysics and Computational Sciences) for assistance in processing *STIS* data, and Ralf Napiwotzki (Dr. Remeis-Sternwarte Bamberg Astronomical Institute of the University of Erlangen-Nürnberg) for useful discussions relating to planetary nebulae and their interaction with white dwarf stars.

REFERENCES

- Abbott D. C., 1982, *Ap.J.*, 259, 282
 Barstow M. A., Dobbie P. D., Holberg J. B., Hubeny I., Lanz T., 1997, *Mon. Not. R. Astr. Soc.*, 286, 58
 Barstow M. A., Holberg J. B., Koester D., 1995, *Mon. Not. R. Astr. Soc.*, 274, L31
 Barstow M. A., Hubeny I., 1998, *Mon. Not. R. Astr. Soc.*, 299, 379
 Barstow M. A., Hubeny I., Holberg J. B., 1999, *Mon. Not. R. Astr. Soc.*, 307, 884
 Barstow, M. A. et al., 1994a, *Mon. Not. R. Astr. Soc.*, 267, 647
 Barstow, M. A. et al., 1994b, *Mon. Not. R. Astr. Soc.*, 271, 175
 Barstow, M. A. et al., 1996, *Mon. Not. R. Astr. Soc.*, 279, 1120
 Barstow, M. A. et al., 2001, in Shipman H., Provencal J., eds, *Proceedings of the 12th European White Dwarfs Workshop Heavy elements in DA white dwarfs*. ASP Conf. Series, pp 128–134
 Barstow, M.A. et al., 2001, *Mon. Not. R. Astr. Soc.*, 325, 1149
 Bohlin R. C., Colina L., Finley D. S., 1995, *Astron. J.*, 110, 1316
 Bruhweiler F., Barstow M., Holberg J., Sahu M., 1999, in *American Astronomical Society Meeting Vol. 195, The Unusual C IV Absorption in the Spectrum of the DA White Dwarf G191-B2B*. pp 3602
 Bruhweiler F. C., Kondo Y., 1982, *Ap.J.*, 259, 232
 Bruhweiler F. C., Kondo Y., 1983, *Ap.J.*, 269, 657
 Chayer P., Fontaine G., Wesemael F., 1995, *Ap.J. (Supp.)*, 99, 189
 Chayer, P. et al., 1995, *Ap.J.*, 454, 429
 Chayer, P. et al., 2000, *Ap.J. (Letters)*, 538, L91
 Dahn, C. C. et al., 1988, *Astron. J.*, 95, 237
 Dgani R., Soker N., 1998, *Ap.J.*, 495, 337
 Dickey J. M., Lockman F. J., 1990, *An. Rev. Astron. Astrophys.*, 28, 215
 Dreizler S., Schuh S., 2001, in Shipman H. L., Provencal J. L., eds, *Proceedings of the 12th European White Dwarf Workshop Stratified non-LTE model atmospheres for hot white dwarfs*. ASP Conf. Series, pp 69–78
 Driebe T., Schoenberner D., Bloeker T., Herwig F., 1998, *Astron. Astrophys.*, 339, 123
 Dupree A. K., Raymond J. C., 1982, *Ap.J. (Letters)*, 263, L63
 Dupree A. K., Raymond J. C., 1983, *Ap.J. (Letters)*, 275, L71
 Dupuis J., Chayer P., Vennes S., Christian D. J., Kruk J. W., 2000, *Ap.J.*, 537, 977
 Finley D. S., Koester D., Basri G., 1997, *Ap.J.*, 488, 375
 Frisch P. C., York D. G., 1983, *Ap.J. (Letters)*, 271, L59
 Fruscione, A. et al. 1994, *Ap.J. (Supp.)*, 94, 127
 Green P. J., Ali B., Napiwotzki R., 2000, *Ap.J.*, 540, 992
 Greenstein J. L., 1984, *Ap.J.*, 276, 602
 Grevesse, N., Sauval, A. J., 1998, *Sp. Sci. Rev.*, 85, 161
 Heber, U., Napiwotzki, R., Lemke, M., Edelman, H., 1997, *Astron. Astrophys.*, 324, L53
 Holberg J. B., Barstow M. A., Bruhweiler F. C., Collins J., 1996, *Astron. J.*, 111, 2361
 Holberg J. B., Barstow M. A., Bruhweiler F. C., Hubeny I., 2000, *American Astronomical Society Meeting*, 197, 0
 Holberg J. B., Barstow M. A., Green E. M., 1997, *Ap.J. (Letters)*, 474, L127
 Holberg J. B., Barstow M. A., Lanz T., Hubeny I., 1997, *Ap.J.*, 484, 871
 Holberg J. B., Barstow M. A., Sion E. M., 1997, in *The Third Conference on Faint Blue Stars Photospheric and Non-Photospheric Features in the Spectra of Hot White Dwarfs*. pp 331
 Holberg J. B., Barstow M. A., Sion E. M., 1998, *Ap.J. (Supp.)*, 119, 207
 Holberg J. B., Barstow M. A., Sion E. M., 1999, in *ASP Conf. Ser. 169: 11th European Workshop on White Dwarfs Elemental abundances in hot white dwarfs*. pp 485
 Holberg J. B., Bruhweiler F. C., Andersen J., 1995, *Ap.J.*, 443, 753
 Holberg J. B., Bruhweiler F. C., Barstow M. A., Dobbie P. D., 1999a, *Ap.J.*, 517, 841
 Holberg J. B., Bruhweiler F. C., Barstow M. A., Dobbie

- P. D., 1999b, in American Astronomical Society Meeting Vol. 195, Probing the Local ISM with Hot White Dwarfs. pp 7201
- Holberg, J. B. et al., 1999, *Ap.J.*, 517, 850
- Holberg, J. B. et al., 2002, American Astronomical Society Meeting, 200, 0
- Kun M., 1998, *Ap.J. (Supp.)*, 115, 59
- Lallement, R. et al., 1995, *Astron. Astrophys.*, 304, 461
- Langill P. P., Kwok S., Hrivnak B. J., 1994, *Publ. Astron. Soc. Pacific*, 106, 736
- MacDonald J., 1992, *Ap.J.*, 394, 619
- Marsh, M. C. et al., 1997, *Mon. Not. R. Astr. Soc.*, 286, 369
- Napiwotzki R., 1999, *Astron. Astrophys.*, 350, 101
- Napiwotzki R., Schönberner D., 1995, *Ap.J.*, 301, 545
- Paresce F., 1984, *Astron. J.*, 89, 1022
- Saffer R. A., Livio M., Yungelson L. R., 1998, *Ap.J.*, 502, 394
- Sahu, M. S. et al., 1999, *Ap.J. (Letters)*, 523, L159
- Schuh S., Dreizler S., 2001, in Shipman H. L., Provencal J. L., eds, Proceedings of the 12th European White Dwarf Workshop Application of stratified non-LTE model atmospheres to hot DA white dwarfs. ASP Conf. Series, pp 79–84
- Sion E. M., Holberg J. B., Barstow M. A., Scheible M. P., 1997, *Astron. J.*, 113, 364
- Tweedy R. W., Kwitter K. B., 1994, *Ap.J. (Letters)*, 433, L93
- Tweedy R. W., Napiwotzki R., 1994, *Astron. J.*, 108, 978
- Unglaub K., Bues I., 2000, *Astron. Astrophys.*, 359, 1042
- Vennes S. ., Lanz T., 2001, *Ap.J.*, 553, 399
- Vennes S., Chayer P., Hurwitz M., Bowyer S., 1996, *Ap.J.*, 468, 898
- Vennes S., Thejll P., Shipman H. L., 1991, in White Dwarfs Abundances of trace heavy elements in hot DA white dwarfs. pp 235
- Vennes S., Thorstensen J. R., 1994, *Astron. J.*, 108, 1881
- Vidal-Madjar, A. et al., 1998, *Astron. Astrophys.*, 338, 694
- Wegner G., 1974, *Mon. Not. R. Astr. Soc.*, 166, 271
- Weinberger R., 1989, *Astron. Astrophys. (Supp.)*, 78, 301
- Wolff B., Koester D., Dreizler S., Haas S., 1998, *Astron. Astrophys.*, 329, 1045
- Wolff B., Jordan S., Koester D., Reimers D., 2000, *Astron. Astrophys.*, 361, 629
- Wolff, B. et al., 2001, *Astron. Astrophys.*, 373, 674
- Wood M. A., 1995, in Lecture Notes in Physics Vol. 443: White Dwarfs Theoretical white dwarf luminosity functions: DA models. pp 41
- Zuckerman B., Reid I. N., 1998, *Ap.J. (Letters)*, 505, L143